

Study of Optical Effects Due to an Induced Polarization Third Order in the Electric Field Strength

P. D. MAKER AND R. W. TERHUNE

Scientific Laboratory, Ford Motor Company, Dearborn, Michigan

(Received 19 August 1964)

This paper presents the results of a series of experiments in which a giant pulsed ruby laser is used to study several different nonlinear optical effects arising from an induced optical polarization third order in the electric field strength. The various phenomena studied are special cases of either frequency mixing or intensity-dependent changes in the complex refractive index, including Raman laser action at a focus. A wide range of crystalline and isotropic materials was studied. The theory for these effects is extended to cover resonant interactions. The experimental results are interpreted in terms of simplified models, and quantitative values for the nonlinear polarizability coefficients are given. The rather large experimental uncertainties in these coefficients are discussed.

I. INTRODUCTION

THIS paper presents the results of several different experiments in which a giant pulsed ruby laser was used to study nonlinear optical effects which can be associated with an induced polarization third order in the electric field strength. These include optical third harmonic generation, electric field induced second harmonic generation, resonant and nonresonant mixing of waves at three different frequencies, intensity dependent changes in the complex index of refraction and Raman laser action.

Several papers on the theory of these effects have been published.¹⁻¹⁶ We have chosen to base our interpretation upon that developed by Armstrong, Bloembergen, Ducuing, and Pershan,¹ which is extended here to include resonant effects. In this framework, each of the experiments measures some component of the same nonlinear, complex, electric susceptibility tensor. The set of experiments, involving a wide range of different frequencies, provides information about the spectral behavior of this tensor.

The first two sections of the paper summarize this theory and apply it with simplifying assumptions to the special cases which correspond to the experiments. These sections are kept brief, as the work to be reported is primarily experimental.

The various experiments are described in the third

section. Measurements were made in a range of liquids, in several cubic crystals, and in an assortment of other crystals and glasses. Often, the description of an interaction involved more than one component of the nonlinear susceptibility tensor. Relative values for these components were deduced, whenever feasible, by studying the interaction as a function of the state of polarization and direction of propagation of the input beam. Also included in this section is a review of our observations of some of the many effects accompanying Raman laser action at the focus of a laser beam.

This study was carried out over an extended period of time and in an exploratory manner. Also, the different experiments made different demands upon the physical properties of the sample. For these reasons, only a few materials were studied in more than one experiment.

II. THE INDUCED POLARIZATION THIRD ORDER IN THE ELECTRIC FIELD STRENGTH

A. Spatial Symmetry Limitations

It will be assumed that in a nonlinear material the induced electric polarization third order in the electric field strength can be expressed as follows:

$$\mathbf{P}^{(3)}(\mathbf{r}, t) = \chi_3 : \mathbf{E}(\mathbf{r}, t) \mathbf{E}(\mathbf{r}, t) \mathbf{E}(\mathbf{r}, t) + (\text{similar terms involving time derivative operators}). \quad (1)$$

This equation must remain invariant to those spatial-symmetry operations which transform the material into itself.¹⁷ Considering only the first term, this implies the following relations, where the nonvanishing components of χ_3 are represented with c 's having the numerical subscripts 1, 2, and 3 for x , y and z , respectively. For isotropic materials

$$P_i^{(3)} = 3c_{1122} E_i (\mathbf{E} \cdot \mathbf{E}). \quad (2)$$

For crystals having point symmetry 432, $\bar{4}3m$, or $m3m$ (NaCl, LiF, CsCl)

$$P_i^{(3)} = 3c_{1122} E_i (\mathbf{E} \cdot \mathbf{E}) + (c_{1111} - 3c_{1122}) E_i^3, \quad (3)$$

¹⁷ R. R. Briss, Proc. Phys. Soc. (London) **79**, 946 (1962).

¹ J. A. Armstrong, N. Bloembergen, J. Ducuing, and P. S. Pershan, Phys. Rev. **127**, 1918 (1962).

² N. Bloembergen and P. S. Pershan, Phys. Rev. **128**, 606 (1962).

³ N. Bloembergen, Proc. IEEE **51**, 124 (1963).

⁴ N. Bloembergen and Y. R. Shen, Phys. Rev. **133**, A37 (1964).

⁵ P. S. Pershan, Phys. Rev. **130**, 919 (1963).

⁶ D. A. Kleinman, Phys. Rev. **125**, 87 (1962).

⁷ D. A. Kleinman, Phys. Rev. **128**, 1761 (1962).

⁸ D. A. Kleinman, Phys. Rev. **126**, 1977 (1962).

⁹ P. A. Franken and J. F. Ward, Rev. Mod. Phys. **35**, 23 (1963).

¹⁰ R. W. Hellwarth, Appl. Opt. **2**, 847 (1963).

¹¹ R. W. Hellwarth, Phys. Rev. **130**, 1850 (1963).

¹² P. N. Butcher and T. P. McLean, Proc. Phys. Soc. (London) **83**, 579 (1964).

¹³ P. N. Butcher and T. P. McLean, Proc. Phys. Soc. (London) **81**, 219 (1963).

¹⁴ M. Goppert-Mayer, Ann. Physik **9**, 273 (1931).

¹⁵ P. L. Kelly, Phys. Chem. Solids **24**, 607 (1963).

¹⁶ R. W. Terhune, Solid State Design **4**, 38 (1963).

where the reference axes correspond to the cubic axes. For crystals having point symmetry 32 (quartz), $3m$ or $\bar{3}m$ (calcite)

$$\begin{aligned} P_x^{(3)} &= 3c_{1122}E_x(E_x^2 + E_y^2) \\ &\quad + 3c_{1133}E_xE_z^2 + 3c_{1311}E_z(E_x^2 - E_y^2), \\ P_y^{(3)} &= 3c_{1122}E_y(E_x^2 + E_y^2) \\ &\quad + 3c_{1133}E_yE_z^2 - 6c_{1311}E_xE_yE_z, \quad (4) \\ P_z^{(3)} &= 3c_{3311}E_z(E_x^2 + E_y^2) \\ &\quad + c_{3333}E_z^3 + c_{3111}(E_x^3 - 3E_y^2E_x), \end{aligned}$$

where the z reference axis corresponds to the threefold symmetry axis and y corresponds to the twofold axis or to the reflection-plane normal.

Next these relations will be considered in terms of the Fourier components of $\mathbf{E}(\mathbf{r}, t)$ and $\mathbf{P}(\mathbf{r}, t)$. The electric field will be assumed to be made up of several harmonic components all of which are plane waves traveling in the \mathbf{r} direction, and written

$$\mathbf{E}(\mathbf{r}, t) = \sum_{j=-N}^N \frac{\mathbf{E}(\omega_j, \mathbf{r})}{2} \exp i(k_j r - \omega_j t), \quad (5)$$

where $\omega_{-j} \equiv -\omega_j$, $k_{-j} \equiv -k_j$ and $\mathbf{E}(\omega_{-j}, \mathbf{r}) \equiv \mathbf{E}^*(\omega_j, \mathbf{r})$. The amplitude function $\mathbf{E}(\omega_j, \mathbf{r})$ here has been assumed to be a slowly varying function of \mathbf{r}_j to account for nonlinear effects. $\mathbf{P}^{(3)}(\mathbf{r}, t)$ will also be assumed expandable in terms of its harmonic components and written

$$\mathbf{P}^{(3)}(\mathbf{r}, t) = \sum_{k=-M}^M \frac{\mathbf{P}(\omega_k, \mathbf{r})}{2} \exp(-i\omega_k t). \quad (6)$$

From Eq. (1) one can derive the following relation between these components

$$\begin{aligned} P_i^{(3)}(\omega_1, \mathbf{r}) &= D\chi_{3lmno}(-\omega_1, \omega_2, \omega_3, \omega_4)E_m(\omega_2, \mathbf{r}) \\ &\quad \times E_n(\omega_3, \mathbf{r})E_o(\omega_4, \mathbf{r})\exp i(k_2 + k_3 + k_4)r, \quad (7) \end{aligned}$$

where $\omega_1 = \omega_2 + \omega_3 + \omega_4$, remembering that both positive and negative frequencies are allowed. This relation, in general, couples together four Fourier components whose positive frequencies satisfy either $\omega_i = \omega_j + \omega_k + \omega_l$ or $\omega_i + \omega_j = \omega_k + \omega_l$. As a result of the terms in Eq. (1) which involve time derivative operators, χ_3 is a function of all four of the frequencies involved. The ordering of the frequencies in the expression $\chi_{3lmno}(-\omega_1, \omega_2, \omega_3, \omega_4)$ is thus not arbitrary. The ordering of the electric fields in (7), however, is unimportant. Thus, the last three frequencies in the χ_3 expression may be interchanged at will provided that the coordinate indices are interchanged in the same manner. Each *distinct* permutation of the electric field vectors in the product $\mathbf{E}(\omega_2, \mathbf{r})\mathbf{E}(\omega_3, \mathbf{r})\mathbf{E}(\omega_4, \mathbf{r})$ contributes to the polarization. In Eq. (7) the ordering has been specified and the factor D inserted into the relation so that coefficients occurring in cases having different frequency degeneracies will have the same weight. In the nondegenerate case $D \equiv 6$.

Further, it has been shown that for lossless materials all four frequencies and coordinate indices of χ_3 can be permuted.^{1,5} Also, for lossless materials, χ_3 is real since Eq. (1) must be invariant under time reversal.

The reader is cautioned that $\chi_{3lmno}(-\omega_1, \omega_2, \omega_3, \omega_4)$ has been defined in Eq. (7) to be one fourth that which one would derive from Eq. (1). With this definition no multiplicative factors are involved for third-harmonic generation when all frequencies on the right-hand side of Eq. (7) are the same. When dc fields are involved, twice their value should be used in Eq. (7).

In terms of Fourier components the induced nonlinear polarization responsible for third-harmonic generation in isotropic materials becomes

$$\begin{aligned} P_i^{(3)}(3\omega, \mathbf{r}) &= 3c_{1122}(-3\omega, \omega, \omega, \omega)E_i(\omega, \mathbf{r}) \\ &\quad \times E_j(\omega, \mathbf{r})E_j(\omega, \mathbf{r})\exp i3k_\omega r. \quad (8) \end{aligned}$$

The equation for the induced nonlinear polarization at ω with only the wave at frequency ω present becomes, in an isotropic material,

$$\begin{aligned} P_i^{(3)}(\omega, \mathbf{r}) &= 6c_{1122}(-\omega, \omega, \omega, -\omega)E_i(\omega, \mathbf{r}) \\ &\quad \times E_j(\omega, \mathbf{r})E_j^*(\omega, \mathbf{r})\exp ik_\omega r \\ &\quad + 3c_{1221}(-\omega, \omega, \omega, -\omega)E_j(\omega, \mathbf{r}) \\ &\quad \times E_j(\omega, \mathbf{r})E_i^*(\omega, \mathbf{r})\exp ik_\omega r. \quad (9) \end{aligned}$$

An additional constant is introduced here reflecting the contribution from the terms in Eq. (1) which involve time derivatives. If the major contribution to χ_3 comes from electronic resonances whose frequencies are much greater than ω , one would expect $c_{1122}(-\omega, \omega, \omega, -\omega) = c_{1221}(-\omega, \omega, \omega, -\omega) = c_{1122}(-3\omega, \omega, \omega, \omega)$. This is equivalent to the statement that the dominant contribution comes from the first term in Eq. (1). As will be shown later, this is true only in special cases since resonances in the differences of frequencies must also be considered. For simplicity, the frequency dependence of the c 's will not be stated in equations in which the induced polarization and the Fourier components of the electric field appear. In these cases, the frequency dependence of c will be given as $c(-\omega_p, \omega_2, \omega_3, \omega_4)$ where ω_p is the frequency of the induced polarization and $\omega_2, \omega_3,$ and ω_4 are the frequencies of the first, second, and third unstarred electric field components taken in the order in which they appear in the equation. Negative frequencies are introduced through the convention defined earlier, $\mathbf{E}^*(\omega, \mathbf{r}) \equiv \mathbf{E}(-\omega, \mathbf{r})$.

The following is the equation for the part of $\mathbf{P}^{(3)}(\omega - \Delta, \mathbf{r})$ due to the presence of $\mathbf{E}(\omega, \mathbf{r})$ and $\mathbf{E}(\omega - \Delta, \mathbf{r})$ in an isotropic material.¹⁸

$$\begin{aligned} P_i^{(3)}(\omega - \Delta, \mathbf{r}) &= 6c_{1122}E_i(\omega - \Delta, \mathbf{r})E_j(\omega, \mathbf{r})E_j^*(\omega, \mathbf{r})\exp ik_{\omega - \Delta} r \\ &\quad + 6c_{1212}E_j(\omega - \Delta, \mathbf{r})E_i(\omega, \mathbf{r})E_j^*(\omega, \mathbf{r})\exp ik_{\omega - \Delta} r \\ &\quad + 6c_{1221}E_j(\omega - \Delta, \mathbf{r})E_j(\omega, \mathbf{r})E_i^*(\omega, \mathbf{r})\exp ik_{\omega - \Delta} r. \quad (10) \end{aligned}$$

¹⁸ L. D. Landau, E. M. Lifshitz, *Electrodynamics of Continuous Media* (Pergamon Press Inc., New York, 1960), p. 381.

One other specialized relation needed to describe the experiments is that which gives the part of $\mathbf{P}^{(3)}(\omega + \Delta, \mathbf{r})$ induced by the presence of $\mathbf{E}(\omega)$ and $\mathbf{E}(\omega - \Delta)$ in isotropic materials:

$$P_i^{(3)}(\omega + \Delta, \mathbf{r}) = 6c_{1122}E_i(\omega, \mathbf{r})E_j(\omega, \mathbf{r}) \times E_j^*(\omega - \Delta, \mathbf{r})\exp i(2k_\omega - k_{\omega - \Delta})r + 3c_{1221}E_j(\omega, \mathbf{r})E_j(\omega, \mathbf{r}) \times E_i^*(\omega - \Delta, \mathbf{r})\exp i(2k_\omega - k_{\omega - \Delta})r. \quad (11)$$

Equations (8), (9), (10), and (11) can be made applicable to the named cubic crystals by adding to each a term, with the appropriate degeneracy factor, of the form $6(c_{1111} - c_{1122} - c_{1221} - c_{1212})E_i(\omega_3, \mathbf{r})E_i(\omega_3, \mathbf{r}) \times E_i(\omega_4, \mathbf{r})\exp i(k_2 + k_3 + k_4)r$. As in (3), the reference axes must now coincide with the cube axes. In the case of plane polarized radiation in cubic crystals, Eq. (9), for instance, may further be written

$$P_i^{(3)}(\omega, \mathbf{r}) = [(6c_{1122} + 3c_{1221})\cos\theta + 3(c_{1111} - 2c_{1122} - c_{1221})\cos^3\theta] \times E^2(\omega, \mathbf{r})E^*(\omega, \mathbf{r})\exp ik_\omega r, \quad (12)$$

where $\cos\theta$ is the i th direction cosine of $\mathbf{E}(\omega, \mathbf{r})$ and $E(\omega, \mathbf{r})$ is the vector amplitude of $\mathbf{E}(\omega, \mathbf{r})$.

B. Frequency Dependence

Armstrong *et al.*¹ have written out the expression for the induced dipole moment per atom (or molecule) to third order using time-dependent perturbation theory and the dipole approximation in a lossless medium. Each of the twenty-four terms which occur in the resulting expression for χ_3 contain three energy denominators. Two of these denominators involve only one of the frequencies contained in the spectrum of the electric field. χ_3 effects associated with resonances in either of these two denominators reflect the intensity dependence of corresponding first order resonances. The third denominator involves two of the frequencies contained in the electric field spectrum. To become resonant, this denominator requires an excited state which has the same parity as the ground state and which is separated from the ground state by the sum or difference of the two frequencies. Effects associated with resonance of this denominator correspond to simultaneous absorption of two photons or absorption of one photon with the simultaneous emission of another at a different frequency. The latter process is the Raman effect.

We have repeated the third-order perturbation development assuming the various energy differences to be complex, i.e., that $\hbar\omega_a = \hbar(\omega_a' - i\Gamma_a)$ where $\hbar\omega_a'$ is the energy and Γ_a the width of the system's a th state. This provides expressions which can be used in the region of resonance. As discussed by Armstrong *et al.*,¹

it is then assumed that the induced polarization per unit volume is equal to the particle density N times the induced dipole moment per particle times a factor $L(-\omega_1, \omega_2, \omega_3, \omega_4)$ which relates the applied macroscopic field to the field acting on the individual particles. This local field-correction factor is of the order $\prod_{j=1}^4 \times \{[\epsilon(\omega_j) + 2]/3\}$ and gives rise to unusually large χ_3 effects in high refractive index materials.

The resonant behavior of the third-order-induced polarization associated with two-photon processes will now be considered in a spectral region away from all linear absorption or resonances in the individual frequencies. To begin with, only one resonant transition will be considered with only a single-frequency component present. Dividing the expression obtained by perturbation theory into a nonresonant and a resonant part, and incorporating the local field correction terms into χ_3 , one obtains

$$P_i^{(3)}(\omega, \mathbf{r}) = 3\chi_{3lmno}(-\omega, -\omega, \omega, \omega)E_m^*(\omega, \mathbf{r}) \times E_n(\omega, \mathbf{r})E_o(\omega, \mathbf{r})\exp ik_\omega r, \quad (13)$$

where

$$3\chi_{3lmno}(-\omega, -\omega, \omega, \omega) \equiv 3\chi_3^{nr}{}_{lmno}(-\omega, -\omega, \omega, \omega) + \frac{1}{2}\chi_3^t{}_{lmno}(-\omega, -\omega, \omega, \omega) \frac{\Gamma_t}{\omega_t' - 2\omega - i\Gamma_t}$$

with

$$\chi_3^t{}_{lmno}(\omega_1, \omega_2, \omega_3, \omega_4) \equiv \frac{NL}{4\hbar\Gamma_t} \langle g | \alpha_{lm}(\omega_1, \omega_2) | t \rangle \langle g | \alpha_{no}(-\omega_3, -\omega_4) | t \rangle^*$$

and

$$\langle g | \alpha_{lm}(\omega_i, \omega_j) | t \rangle \equiv \frac{e^2}{\hbar} \sum_b \left(\frac{\langle g | x_l | b \rangle \langle b | x_m | t \rangle}{\omega_b' + \omega_i} + \frac{\langle g | x_m | b \rangle \langle b | x_l | t \rangle}{\omega_b' + \omega_j} \right),$$

where g and t refer to the ground and resonant states and $\hbar\omega_b'$ is the energy of the intermediate state b . We will be concerned with two photon absorption, as characterized by the second term of Eq. (13), to electronic states in solids and liquids having half-widths $\Gamma_t/\pi c$ of a few hundred wave numbers. Assuming a value of 10^{-24} cm³ for the polarizability matrix elements for these transitions, $\langle g | \alpha_{lm}(\omega_i, \omega_j) | t \rangle$, one predicts a value of the order of 10^{-13} cm³ erg⁻¹ for χ_3^t .

Next the case with two frequency components ω and $\omega - \Delta$ present will be considered. A Raman resonance transition near the frequency difference Δ will be assumed in addition to one near the sum frequency $2\omega - \Delta$. The nonlinear polarization at the frequency $\omega - \Delta$ due to the presence of both frequencies would be given by the following:

$$P_i^{(3)}(\omega - \Delta, \mathbf{r}) = 6\chi_{3lmno}[-(\omega - \Delta), \omega, \omega - \Delta, -\omega]E_m(\omega, \mathbf{r})E_n(\omega - \Delta, \mathbf{r})E_o^*(\omega, \mathbf{r})\exp ik_{\omega - \Delta} r, \quad (14)$$

where

$$6\chi_{3lmno}[-(\omega-\Delta),\omega,\omega-\Delta,-\omega] \equiv 6\chi_{3nr}{}_{lmno}[-(\omega-\Delta),\omega,\omega-\Delta,-\omega] \\ + \chi_{3r}{}_{lmno}[-(\omega-\Delta),\omega,\omega-\Delta,-\omega] \frac{\Gamma_r}{\omega_r' - \omega + (\omega-\Delta) + i\Gamma_r} + \chi_{3t}{}_{lonm}[-(\omega-\Delta),-\omega,\omega-\Delta,\omega] \frac{\Gamma_t}{\omega_t' - \omega - (\omega-\Delta) - i\Gamma_t},$$

with

$$\chi_{3r}{}_{lmno}(\omega_1,\omega_2,\omega_3,\omega_4) \\ \equiv (NL/4\hbar\Gamma_r) \langle g|\alpha_{lm}(-\omega_1,-\omega_2)|r\rangle^* \\ \times \langle g|\alpha_{no}(\omega_3,\omega_4)|r\rangle,$$

and $\chi_{3t}{}_{lonm}(-(\omega-\Delta),-\omega,\omega-\Delta,\omega)$ and $\langle g|\alpha_{lm}(\omega_1,\omega_2)|r\rangle$ as defined earlier. Here, the subindices and frequencies of χ_{3t} have been permuted so that the definition given in Eq. (13) gives the correct resonance expression. The term proportional to χ_{3r} , will, in the next section, be associated with the coherent Raman effect or Raman laser action. Its resonance denominator derives from an expression involving ω_r^* and hence contains $+i\Gamma_r$. The spontaneous emission associated with this term gives rise to the conventional Raman effect. Thus the data from molecular rotation-vibration Raman spectra can be used to determine χ_{3r} and Γ_r . The major contribution to the intensity of the strongest vibrational Raman transitions in liquids comes from the isotropic part of $\langle g|\alpha|r\rangle$ denoted in the literature by α_{01} where the subindices are the initial and final vibrational quantum numbers. Spectroscopic results are usually expressed in terms of α' , the derivative of the polarizability matrix element with respect to the normal coordinate involved in the transition, where $\alpha'^2 = (2\omega/\hbar)\alpha_{01}^2$ with ω the frequency of the transition.¹⁹ Quantitative Raman scattering data give $L\alpha'^2 = 2.9 \pm 0.3 \times 10^{-9} \text{ cm}^4 \text{ g}^{-1}$ for the 459-cm⁻¹ line of gaseous CCl₄ and $7.5 \pm 2 \times 10^{-9} \text{ cm}^4 \text{ g}^{-1}$ for the liquid.²⁰ In passing, this implies $L_{liq}/L_{gas} = 2.6 \pm 0.8$ while $((\epsilon_{liq} + 2)/3)^4 = 2.6$. The ratio of the intensities of the benzene 992 cm⁻¹ Raman line and the 459 cm⁻¹ CCl₄ line is 4.92 for liquid samples.²¹ This ratio is given by

$$\frac{N_b L_b \alpha_{b01}^2 [(\omega - \Delta_b)]^4 \epsilon_b(\omega - \Delta_b) \epsilon_c(\omega)}{N_c L_c \alpha_{c01}^2 [(\omega - \Delta_c)]^4 \epsilon_c(\omega - \Delta_c) \epsilon_b(\omega)},$$

$$P_l^{(3)}(\omega + \Delta, r) = 3\chi_{3lmno}[-(\omega + \Delta), \omega, \omega, -(\omega - \Delta)] E_m(\omega, r) E_n(\omega, r) E_0^*(\omega - \Delta, r) \exp i(2k_\omega - k_{\omega - \Delta})r, \quad (15)$$

where

$$3\chi_{3lmno}[-(\omega + \Delta), \omega, \omega, -(\omega - \Delta)] \equiv 3\chi_{3nr}{}_{lmno}[-(\omega + \Delta), \omega, \omega, -(\omega - \Delta)] \\ + \chi_{3r}{}_{lmno}[-(\omega + \Delta), \omega, \omega, -(\omega - \Delta)] \frac{\Gamma_r}{\omega_r' - \omega + (\omega - \Delta) - i\Gamma_r} + \frac{1}{2}\chi_{3t}{}_{lonm}[-(\omega + \Delta), -(\omega - \Delta), \omega, \omega] \frac{\Gamma_t}{\omega_t' - \omega - \omega - i\Gamma_t}.$$

where N_b and N_c are the particle densities, $L_c^{1/2}\alpha_{b01}$ and $L_c^{1/2}\alpha_{c01}$ are the local field-corrected polarizability matrix elements, Δ_b and Δ_c are the Raman displacement frequencies, $\epsilon_b(\omega_i)$ and $\epsilon_c(\omega_i)$ are the dielectric constants at ω_i of benzene and CCl₄, respectively, and ω is the frequency of the exciting source. Thus $L_b\alpha_{b01}^2 = 2.0 \pm 0.5 \times 10^{-49} \text{ cm}^6$. Using a ruby laser source, McClung and Weiner²² have recently made quantitative Raman scattering measurements for the 992 cm⁻¹ benzene liquid line, expressing their results in terms of a scattering cross section. Using the relation

$$\sigma_{\omega,\Omega} d\omega d\Omega = \frac{NL\alpha_{01}^2 [(\omega - \Delta)]^4 \epsilon(\omega - \Delta) \Gamma}{c^4 \epsilon(\omega) \pi \Delta\omega^2 + \Gamma^2} \frac{d\omega}{\Delta\omega^2 + \Gamma^2} \sin^2\theta d\Omega,$$

where $\sigma_{\omega,\Omega}$ is the scattering cross section per cm per steradian per frequency interval and θ is the angle between the direction of observation and the electric vector of the plane polarized exciter light, their data gives $L_b\alpha_{b01}^2 = 2.1 \pm 0.5 \times 10^{-49} \text{ cm}^6$, in excellent agreement with the earlier measurements. They have also measured the scattered linewidth to be 3.1 cm⁻¹. Using their values,

$$\chi_{3r}{}_{xxxx}[-(\omega_l - \Delta_b), \omega_l, \omega_l - \Delta_b, -\omega_l] \\ = 1.2 \pm 0.3 \times 10^{-12} \text{ cm}^3 \text{ erg}^{-1}, \frac{\omega_l}{2\pi c} = 14\,400 \text{ cm}^{-1}.$$

These two photon processes can also serve to couple waves at four different frequencies. This coupling can be thought of as an interference between two pairs of waves each of which is inducing two photon processes. A special case of this involves the three frequencies $\omega + \Delta$, ω , and $\omega - \Delta$. The additional nonlinear polarization at $\omega + \Delta$ due to the presence of both $\mathbf{E}(\omega, r)$ and $\mathbf{E}(\omega - \Delta, r)$ is, assuming a two photon absorption resonance at 2ω as well as a Raman resonance at Δ ,

¹⁹ T. Yoshino and H. J. Bernstein, J. Mol. Spectr. 2, 241 (1948).

²⁰ H. W. Schrötter and H. J. Bernstein, J. Mol. Spectr. 7, 464 (1961).

²¹ J. P. Jesson and H. W. Thompson, Proc. Roy. Soc. (London) A268, 68 (1962).

²² F. J. McClung and D. Weiner, J. Opt. Soc. Am. 54, 641 (1964).

The coefficients χ_3^r and χ_3^t in this expression are slowly varying functions of the frequencies and, as Δ is small, they will be assumed equal to those in Eqs. (13) and (14). To obtain the total $\mathbf{P}^{(3)}(\omega+\Delta, r)$, one must add to Eq. (15) appropriately modified versions of Eqs. (13) and (14).

III. EFFECTS OF THE NONLINEAR POLARIZATION ON THE PROPAGATION OF ELECTROMAGNETIC WAVES

A. Maxwell's Equation with a Nonlinear Polarization

In this section the induced nonlinear polarization is used as a source term in Maxwell's equations to determine its effect upon the propagation of the various frequency components. Only the special cases needed to interpret the experimental results will be considered. Following the approach used by Armstrong *et al.*¹ and assuming a plane wave in an isotropic medium, except when stated otherwise, one obtains the following set of complex vector equations, one for each frequency component.

$$\frac{d}{dr} E_n(\omega_j, r) = i \frac{2\pi k_{\omega_j}}{\epsilon_{\omega_j}} P_n^{(3)}(\omega_j, r) \exp(-ik_{\omega_j} r). \quad (16)$$

This result is obtained by substituting the expressions (5) and (6) into Maxwell's equations and neglecting second derivatives of the slowly varying amplitude function $\mathbf{E}(\omega_j, r)$. In the following, no consideration will be given the small nonlinear effects which arise in satisfying boundary conditions.² In addition, the various interactions will be considered separately although in practice they occur simultaneously.

B. Intensity-Dependent Effects With a Monochromatic Wave

First the effect of the nonlinear polarization induced by a plane-polarized monochromatic wave upon the wave itself will be considered. From Eqs. (9) and (16)

$$\frac{d}{dr} E(\omega, r) = i \frac{2\pi k_{\omega}}{\epsilon_{\omega}} [6c_{1122} + 3c_{1221}] E^2(\omega, r) E^*(\omega, r). \quad (17)$$

Writing $E(\omega, r) = |E(\omega, r)| \exp i\Phi(\omega, r)$ and $(6c_{1122} + 3c_{1221}) = (6c_{1122} + 3c_{1221})' + i(6c_{1122} + 3c_{1221})''$ we obtain upon equating real and imaginary parts of Eq. (17)

$$\frac{d|E(\omega, r)|}{dr} = \frac{-2\pi k_{\omega}}{\epsilon_{\omega}} (6c_{1122} + 3c_{1221})'' |E(\omega, r)|^3, \quad (18)$$

$$\frac{d\Phi(\omega, r)}{dr} = \frac{2\pi k_{\omega}}{\epsilon_{\omega}} (6c_{1122} + 3c_{1221})' |E(\omega, r)|^2. \quad (19)$$

Equation (18) integrates directly to give^{6,23}

$$\frac{1}{|E(\omega, r)|^2} = \frac{1}{|E(\omega, 0)|^2} + \frac{4\pi k_{\omega}}{\epsilon_{\omega}} (6c_{1122} + 3c_{1221})'' r, \quad (20)$$

where the nonlinear medium is assumed to occupy the half-space $r > 0$. This equation describes the intensity-dependent attenuation of a wave due to two photon absorption. When 2ω is in the region of a two photon resonance frequency, from Eq. (13)

$$(6c_{1122} + 3c_{1221})'' \approx \frac{1}{2} \chi_3^t{}_{xxxx}(-\omega, -\omega, \omega, \omega) \frac{\Gamma_t^2}{(\omega_t - 2\omega)^2 + \Gamma_t^2}.$$

Using (20), Eq. (19) may also be integrated.

In the lossless case, $(6c_{1122} + 3c_{1221})''$ is zero and from Eq. (18) $|E(\omega, r)|$ is constant. Equation (19) then integrates directly and the nonlinear interaction can be expressed as an intensity-dependent change in the index of refraction given by

$$\delta n = (2\pi/n_{\omega})(6c_{1122} + 3c_{1221})' |E(\omega, r)|^2. \quad (21)$$

Let us now consider the more complicated case of elliptically polarized light but restrict the discussion to lossless media. Transforming Eqs. (9) and (17) into a circular representation with $E^+ \equiv (1/\sqrt{2})(E_x + iE_y)$ and $E^- \equiv (1/\sqrt{2})(E_x - iE_y)$ one deduces the following expression for the intensity-dependent refractive index changes for the two senses of circular polarization²⁴

$$\begin{aligned} \delta n^+ &= -\frac{2\pi}{n_{\omega}} [3c'_{1122} |E^+(\omega, r)|^2 \\ &\quad + (3c'_{1122} + 3c'_{1221}) |E^-(\omega, r)|^2], \\ \delta n^- &= -\frac{2\pi}{n_{\omega}} [3c'_{1122} |E^-(\omega, r)|^2 \\ &\quad + (3c'_{1122} + 3c'_{1221}) |E^+(\omega, r)|^2]. \end{aligned} \quad (22)$$

Inspection of (22) shows that with elliptically polarized light incident, the change in index is different for the two senses of circular polarization. Let α be defined as the angle of inclination of the vibrational ellipse of the elliptically polarized radiation, measured from the x toward the $+y$ axis. Then α is equal to one-half the phase difference between $E^+(\omega, r)$ and $E^-(\omega, r)$ and varies with r as follows

$$\begin{aligned} \alpha &= \alpha_0 + \frac{1}{2}(\omega/c)(\delta n^+ - \delta n^-)r \\ &= \alpha_0 + (\pi\omega/n_{\omega}c)3c'_{1221}(|E^-(\omega, r)|^2 - |E^+(\omega, r)|^2)r. \end{aligned} \quad (23)$$

Thus, one predicts an intensity-dependent rotation of the vibrational ellipse with r . The direction of the rotation is determined by the sign of $3c'_{1221}$ and the handedness of the ellipticity.

²³ J. A. Giordmaine and John A. Howe, Phys. Rev. Letters **11**, 207 (1963).

²⁴ P. D. Maker, R. W. Terhune, and C. M. Savage, Phys. Rev. Letters **12**, 507 (1964).

C. Changes in Refractive Index at One Frequency Due to the Presence of a Wave at Another Frequency

Here, only the case with both waves polarized in the same direction in isotropic media will be considered in detail. Substituting Eq. (10) into Eq. (16) one obtains

$$\frac{dE(\omega-\Delta, r)}{dr} = i(2\pi k_{\omega-\Delta}/\epsilon_{\omega-\Delta})6(c_{1122}+c_{1221}+c_{1212}) \times E(\omega-\Delta, r)E(\omega, r)E^*(\omega, r). \quad (24)$$

If the material has a Raman resonance frequency at $\omega'_r = \Delta$, the relation (10) and the resonance expression (14) give, considering only the resonant term,^{16,25}

$$\frac{dE(\omega-\Delta, r)}{dr} = \frac{2\pi k_{\omega-\Delta}}{\epsilon_{\omega-\Delta}} \frac{NL\alpha_{01}^2}{4\hbar\Gamma_r} E(\omega-\Delta, r)E(\omega, r)E^*(\omega, r). \quad (25)$$

When the attenuation of $E(\omega, r)$ can be neglected, this describes amplification of the wave at frequency $\omega-\Delta$ with an amplitude gain per centimeter

$$\frac{\pi k_{\omega-\Delta} NL\alpha_{01}^2}{2\hbar\epsilon_{\omega-\Delta}\Gamma_r} E^*(\omega, r)E(\omega, r).$$

This process is known as Raman laser action. Restricted by our assumption that the waves at ω and $\omega-\Delta$ are plane polarized in the same direction, the gain described by Eq. (25) is independent of the direction of propagation of the two waves. For the more general case in which the wave at ω is elliptically polarized, the gain at $\omega-\Delta$ will depend upon both the state of polarization and relative direction of propagation of the wave at $\omega-\Delta$.

Similarly, if ω'_i is a two-photon resonance frequency of the material and $2\omega-\Delta = \omega'_i$, one obtains

$$\frac{dE(\omega-\Delta, r)}{dr} = -\frac{2\pi k_{\omega-\Delta}}{\epsilon_{\omega-\Delta}} \chi_3^t{}_{xxxx}[-(\omega-\Delta), -\omega, \omega, (\omega-\Delta)] \times E^*(\omega, r)E(\omega, r)E(\omega-\Delta, r), \quad (26)$$

which predicts, when $E(\omega, r)$ can be considered constant, an additional linear loss with an amplitude attenuation coefficient per centimeter of

$$(2\pi k_{\omega-\Delta}/\epsilon_{\omega-\Delta})\chi_3^t{}_{xxxx}[-(\omega-\Delta), -\omega, \omega, (\omega-\Delta)] \times E(\omega, r)E^*(\omega, r).$$

We shall also need an expression for the birefringence induced at $\omega-\Delta$ by the presence of a wave at ω . Far from all resonances, and with the wave at ω plane polarized, the changes in the refractive index at $\omega-\Delta$ for $\mathbf{E}(\omega-\Delta, r)$ perpendicular and parallel to $\mathbf{E}(\omega, r)$ from Eq. (10) are

$$\delta n^\perp = (2\pi/n_{\omega-\Delta})6c_{1122}E(\omega, r)E^*(\omega, r),$$

$$\delta n^\parallel = (2\pi/n_{\omega-\Delta})6(c_{1122}+c_{1221}+c_{1212})E(\omega, r)E^*(\omega, r). \quad (27)$$

²⁵ R. W. Minck, R. W. Terhune, and W. G. Rado, Appl. Phys. Letters 3, 181 (1963).

D. Creation of New Frequency Components

For the case of optical third-harmonic generation, Eqs. (8) and (16) result in the expression,

$$\frac{dE(3\omega, r)}{dr} = i\frac{2\pi k_{3\omega}}{\epsilon_{3\omega}} 3c_{1122}E^3(\omega, r)\exp i(3k_\omega - k_{3\omega})r. \quad (28)$$

Assuming $E(\omega, r)$ constant, this equation integrates directly to give

$$E(3\omega, r) = \frac{2\pi k_{3\omega}}{\epsilon_{3\omega}} 3c_{1122}E^3(\omega, r) \left[\frac{1 - \exp i\Delta kr}{\Delta k} \right], \quad (29)$$

where $\Delta k \equiv 3k_\omega - k_{3\omega}$. The last term is seen to have a maximum value of $2/\Delta k$ when $\Delta kr = \pi$. This is the well known effect which limits the amount of harmonic generation when, because of dispersion, the phase velocities of the waves are not matched.^{26,27} In the special case $\Delta k = 0$, which requires here that the refractive index of the third-harmonic and fundamental waves be equal, the bracketed term becomes equal to $-ir$. Thus, in the "index matched" case the amplitude of the third-harmonic ray grows linearly with distance. Also, from Eq. (29), the third-harmonic power is proportional to $|c_{1122}|^2$ —both the real and imaginary parts of χ_3 contribute to this and other frequency mixing processes.

A similar equation can be derived for the creation of a wave at $\omega+\Delta$ due to the presence of waves at ω and $\omega-\Delta$ which are plane polarized in the same direction. Thus, from Eqs. (11) and (16), and assuming $E(\omega, r)$ and $E(\omega-\Delta, r)$ constant,

$$E(\omega+\Delta, r) = \frac{2\pi k_{\omega+\Delta}}{\epsilon_{\omega+\Delta}} (6c_{1122} + 3c_{1221}) \times E^2(\omega, r)E^*(\omega-\Delta, r) \left[\frac{1 - \exp i\Delta kr}{\Delta k} \right], \quad (30)$$

where here $\Delta k \equiv 2k_\omega - k_{\omega+\Delta} - k_{\omega-\Delta}$. This process becomes resonant in accordance with Eq. (15).

E. Measured Quantities

The preceding results for isotropic materials may be expressed in terms of the time averaged power at frequency ω , $W(\omega, r)$, using the relation

$$W(\omega, r) = (n_\omega c/8\pi) \mathbf{E}(\omega, r) \cdot \mathbf{E}^*(\omega, r) \mathcal{A}. \quad (31)$$

Here \mathcal{A} is the cross-sectional area of the beam. In analyzing the data, (31) will be used without modification whenever the beam diameter remains essentially constant throughout the sample. In some experiments, however, the beam passed through a focus inside a thick sample. If index matched, it will be assumed that

²⁶ J. A. Giordmaine, Phys. Rev. Letters 8, 19 (1962).

²⁷ P. D. Maker, R. W. Terhune, M. Nisenoff, and C. M. Savage, Phys. Rev. Letters 8, 21 (1962).

the entire interaction occurs within a cylindrical focal volume having a length to cross-sectional area ratio of

$$l/Q = 3.5n/\lambda, \quad (32)$$

within which plane waves are propagating. This model is based upon a rough numerical evaluation of $\int dr/Q(r)$ using the intensity distribution in the region of a diffraction limited focus.²⁸ It predicts that the interaction is independent of the focal length of the imaging system used. Several crude experimental tests have borne out this result. The following are examples of the application of this model. A beam which is brought to a diffraction limited focus entirely within a thick sample is attenuated through two photon absorption according to

$$\begin{aligned} 1/W_t &= 1/W_i + 1/W_m, \\ 1/W_m &= (56\pi k_\omega^2/cn_\omega^3)(6c_{1122} + 3c_{1221})'', \end{aligned} \quad (33)$$

where W_t and W_i are the transmitted and incident power. The vibrational ellipse of a light beam ideally focused inside a sample is rotated an amount α_T given by

$$\alpha_T = (14\pi k_\omega^2/cn_\omega^3)3c'_{1221}(W^- - W^+). \quad (34)$$

The power gain per traversal of an ideal focus for Raman laser action, G_t , assuming the laser beam unattenuated, becomes

$$G_t = \exp\left[\frac{14\pi N L \alpha_0^2 k_\omega k_{\omega-\Delta}}{c\hbar n_\omega^8 \Gamma_r} W(\omega)\right]. \quad (35)$$

In practice, the laser beam did not form a diffraction limited focus. These models were used, however, but with the l/Q ratio degraded by a factor of three which represents our estimate of the effect of this imperfection.

IV. EXPERIMENTAL RESULTS

A. The Laser

A high-optical-quality 90° ruby rod, $\frac{1}{4}$ in. in diameter by 2 in. long and rough ground on the cylinder walls was used. By cooling the rod to -45°C , no coatings were needed on either end. The helical flash lamp was powered by a regulated supply and Q spoiling was accomplished using a motor driven roof prism rotating at 24 000 rpm. The system was fired at regular 30-sec intervals and provided an output pulse of 0.1 J with a nearly triangular pulse shape 30 nsec wide at half-height. The plane polarized output consisted of two parallel beams each ~ 1 mm in diameter and separated by ~ 2 mm. These came to separate foci, some 20% of their total energy being contained in the two diffraction limited focal spots. In practice, only one of the beams was used. This laser was capable of creating dielectric breakdown in air when brought to focus by a 3-cm focal length lens.

²⁸ M. Born, E. Wolf, *Principles of Optics* (Pergamon Press, Inc., New York, 1959), p. 434.

The output beam from the laser, however, was far from ideal. The frequency spread of the radiation was of the order of $\frac{1}{3}$ cm⁻¹. Further, inspection of the output beam with a time swept image intensifier camera showed considerable spatial structure which varied a great deal in times less than 10^{-9} sec. These factors have not been taken into account in our analysis.

B. Optical Harmonic Generation

To study optical third-harmonic generation^{29,30} various samples were placed at or near a focus of the laser beam. A combination NiSO₄-CoSO₄ water filter with quartz windows was placed after the sample. This filter attenuated the laser beam by more than 10^{15} while attenuating the third-harmonic radiation at 2313 Å by about 40. For most of the experiments a grating monochromator was also used to provide further wavelength discrimination. A 1P28 photomultiplier was used to detect the third-harmonic radiation. The signal from this phototube was displayed along with that from a phototube monitoring the laser intensity using a high-speed dual-beam oscilloscope. Polaroid photos of the trace constituted the data.

Equation (29) describes the amplitude growth of the third harmonic wave under nonindex matched conditions. The coherence length $l_{\text{coh}} = \pi/\Delta k$ was computed, using index of refraction data, for several transparent materials and found to be of the order of one micron. In spite of this, third-harmonic signals were detected from many materials by focusing the laser into the samples. At these high intensities, however, dielectric breakdown accompanied by sparking was imminent. Due to this difficulty, reliable data could be obtained for only lithium fluoride, which had both a relatively long coherence length (3.5 μ) and good optical dielectric strength.

A 3-cm-thick lithium fluoride sample was used. It was placed in the laser beam at the focus of a composite lens comprised of a 10-cm focal length spherical and a 50-cm focal length cylindrical lens. This purposely-introduced aberration permitted more efficient use of the available laser power. At a laser power of 10^5 W, a signal of 20 photoelectrons, corresponding to the creation of about 5000 third-harmonic photons, was observed. At slightly higher levels, the sample broke down. This signal was found to vary with the angle θ in a manner consistent with Eqs. (8) and (12) with $[c_{1111}/3c_{1122}](-3\omega_l, \omega_l, \omega_l, \omega_l) = +0.64$ or -0.28 assuming the ratio real. The frequency dependence of the quantity in the square bracket has been noted with ω_l the frequency of the laser. Rough estimates gave

$$|[3c_{1122} + c_{1111}](-3\omega_l, \omega_l, \omega_l, \omega_l)| = 3 \times 10^{-15} \text{ cm}^3 \text{ erg}^{-1}.$$

²⁹ R. W. Terhune, P. D. Maker, and C. M. Savage, *Phys. Rev. Letters* **8**, 404 (1962).

³⁰ P. D. Maker, R. W. Terhune, and C. M. Savage, *Quantum Electronics III*, edited by P. Grivet and N. Bloembergen (Columbia University Press, New York, 1964), p. 1559.

As discussed by several authors, Δk becomes zero for certain interactions at specific directions of propagation through sufficiently birefringent crystals.^{26,27} In calcite $\Delta k = 3k_0(\omega) - k_e(3\omega) = 0$ for the process $P_e^{(3)}(3\omega, z) \propto E_0^3(\omega, z)$ when the crystal optic axis or z axis is inclined at $\theta = 47^\circ$ to the propagation vector $\mathbf{k}(\omega)$. Here $P_e^{(3)}(3\omega, r)$ is the induced polarization parallel to the electric vector of the third-harmonic extraordinary ray and $E_0(\omega, r)$ is the electric vector of the ordinary ray component of the laser beam. Using Eq. (4),

$$P_e^{(3)}(3\omega, r) = c_{3111} E_0^3(\omega, r) \cos 3\varphi \sin(\theta + \alpha_3) \times \exp[i3k_0(\omega)r], \quad (36)$$

where α_n is the angle between $E_e(n\omega, r)$ and $D_e(n\omega, r)$, or between the phase and ray velocities. Here φ , the angle of positive rotation of the crystal about the "z" axis, is zero for \mathbf{x} along $\mathbf{k}(\omega) \times \mathbf{z}$. In identifying the directed crystallographic axes, the rhombohedral cleavage planes of calcite were assumed, as in Winchell,³¹ to be $(10\bar{1}1)$, $(1\bar{1}0\bar{1})$, etc., planes. Here the Bravais-Miller indices refer to the three equivalent y , or twofold, axes and to z , the $\bar{3}$ axis. Figure 1 shows the relative orientation of the crystal, the fields, and the direction of propagation. Also shown is the observed dependence of the third-harmonic generation on φ . This data was obtained by focusing the laser beam into a 4-mm-thick calcite crystal with the z axis normal to the surface. To permit the beam to enter the crystal and propagate at 47° to the z axis, the sample was placed within a glycerine bath. The crystal was rotated around the z axis to vary φ .

Third harmonic can also be generated under index matched conditions with $\Delta k \equiv 2k_0(\omega) + k_e(\omega) - k_e(3\omega) = 0$ for $\theta = 57^\circ$ and the induced polarization may be written

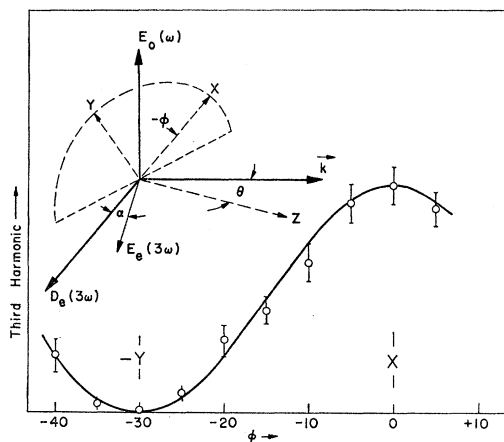


FIG. 1. Observed dependence of the third-harmonic generation in calcite upon φ fitted to the expected dependence $(\cos 3\varphi)^2$. The data were obtained by rotating the crystal around the z axis maintaining θ at 47° .

³¹ A. N. Winchell, *The Microscopic Characters of Artificial Inorganic Solid Substances or Artificial Minerals* (John Wiley & Sons, Inc., New York, 1931).

as follows:

$$P_e^{(3)}(3\omega, r) = \{ [c_{1122} \cos(\theta + \alpha_1) \cos(\theta + \alpha_3) + c_{3311} \sin(\theta + \alpha_1) \sin(\theta + \alpha_3)] + \sin 3\varphi [c_{3111} \sin(\theta + \alpha_3) \cos(\theta + \alpha_1) + c_{1311} \sin(\theta + \alpha_1) \cos(\theta + \alpha_3)] \} \times 3E_0^2(\omega, r) E_e(\omega, r) \exp i[2k_0(\omega) + k_e(\omega)]r. \quad (37)$$

When the laser beam was focused into a 4-mm-thick crystal of calcite at $\theta = 57^\circ$ and $\varphi = \pi/2$, the third harmonic intensity increased to the point where we were able to photograph it using 10 000 speed polaroid film. This signal was found to maximize, as does the product $E_0^3(\omega, r) E_e(\omega, r)$, when the angle between the polarization vector of the incoming beam and the plane containing $\mathbf{k}(\omega)$ and the z axis was $\arctan \sqrt{2}$. The energy conversion efficiency to third harmonic was observed to vary as the square of the laser intensity, as expected, and reached a maximum of 3×10^{-6} with a 1-MW laser pulse. As noted in the following, 2.6 times this conversion efficiency would be expected with $\varphi = -\frac{1}{2}\pi$.

The growth of $E_e(3\omega, r)$ can be calculated using the above formula for $P_e(3\omega, r)$ and Eq. (29) with $\Delta k = 0$. Equation (29) was derived for isotropic media and to relate $E_e(3\omega, r)$ to $P_e(3\omega, r)$ the right-hand side must be divided by $\cos^2 \alpha_3$.¹ However, values for the coefficients obtained from the above experiments are subject to large uncertainties. Besides the complications involved in using a focused beam near index match, one must consider the 5 to 10 deg difference in direction between the phase and ray velocities for the extraordinary rays.⁷ This effect limits the distance over which the ordinary and extraordinary rays can interact to the order of 10 times the diameter of the beam. Thus, a different experimental arrangement was used to evaluate the coefficients.

Thin platelets of calcite properly oriented to obtain third-harmonic generation at normal incidence near each of the above index matching conditions were prepared. Measurements were made of the third harmonic generated in these samples in the unfocused laser beam. Twenty-two times as much signal was obtained from a 0.75-mm-thick sample oriented with $\theta = 57^\circ$, $\varphi = 0$ as from a 0.50-mm-thick sample oriented with $\theta = 47^\circ$, $\varphi = 0$. From this we deduce

$$\left| \frac{c_{3111}}{0.17c_{1122} + 0.83c_{3311}} \right| (-3\omega_l, \omega_l, \omega_l, \omega_l) = 0.20.$$

In calculating the above, no correction for the angular divergence of the laser beam had to be made, as the thickness ratio was chosen equal to the ratio of $(d\Delta k/d\theta)^{-1}$ for the two index matching conditions.⁷

Comparing samples of equal thickness with $\theta = 57^\circ$, 2.6 times as much signal was obtained with $\varphi = -\frac{1}{2}\pi$ as with $\varphi = +\frac{1}{2}\pi$. From this result, assuming the ratio

real,

$$\left[\frac{0.39c_{3111} + 0.36c_{1311}}{0.17c_{1122} + 0.83c_{3311}} \right] (-3\omega_l, \omega_l, \omega_l, \omega_l) = 0.25.$$

From the last two results, which have an accuracy of about $\pm 25\%$, $c_{3111}/c_{1311} = 0.4 \pm 0.3$ or -0.2 ± 0.1 . For crystals transparent throughout the visible to beyond 3ω , and with ω in the visible, one would expect $c_{3111} \approx c_{1311}$.

Measurement of the third harmonic and laser intensities were made to determine the absolute values of the coefficients. To minimize errors due to the angular spread of the laser beam,⁷ a 0.23-mm-thick sample, with $\theta = 57^\circ$, $\varphi = \pi/2$, was used. Aperture stops were used to define the beam cross section. For a 10 mJ, 28-nsec half-width laser pulse having a beam diameter of 2 mm, a 10^{-13} -J third-harmonic pulse with a 20-nsec half-width was observed. The photomultipliers used were calibrated with a bolometer at the laser frequency and its second harmonic. Using Eqs. (29) and (34), and the previously measured ratios,

$$\begin{aligned} |0.17c_{1122} + 0.83c_{3311}| (-3\omega_l, \omega_l, \omega_l, \omega_l) \\ = 2 \times 10^{-15} \text{ cm}^3 \text{ erg}^{-1}. \end{aligned}$$

For comparative purposes, second-harmonic generation in ADP was also measured using the same arrangement, and gave

$$d_{36} = 7 \pm 4 \times 10^{-10} \text{ cm}^3/2 \text{ erg}^{-1/2}.$$

The previously reported values of d_{36} obtained using a ruby laser are 3×10^{-10} for ADP³² and $6 \times 10^{-10} \text{ cm}^3/2 \text{ erg}^{-1/2}$ for KDP⁷ ($\sim 10\%$ higher than ADP).³³ However, the apparently more accurate value obtained with a gas laser³⁴ is $30 \pm 10 \times 10^{-10} \text{ cm}^3/2 \text{ erg}^{-1/2}$. A factor of $\sqrt{2}$ of this difference might be explainable in terms of many independent frequency components present at the same time in the laser beam in one case and not the other.³⁴

Electric-field-induced second-harmonic generation has also been observed in calcite.²⁹ $\Delta k = 2k_0(\omega) - k_e(2\omega) = 0$ for this process with $\theta = 37^\circ$. The dc field \mathbf{E}_{dc} was applied at right angles to $\mathbf{k}(\omega)$ in the plane of the extraordinary ray. The equation describing the nonlinear polarization is in this case

$$\begin{aligned} P_e^{(3)}(2\omega, r) = & [3c_{1122} \cos\theta \cos(\theta + \alpha_2) \\ & + 3c_{3311} \sin\theta \sin(\theta + \alpha_2) \\ & + \sin 3\varphi \{ 3c_{3111} \sin(\theta + \alpha_2) \cos\theta \\ & + 3c_{1311} \cos(\theta + \alpha_2) \sin\theta \}] \\ & \times 2E_0^2(\omega, r) E_{dc} \exp(i2k_0[\omega]r). \quad (38) \end{aligned}$$

With $E_{dc} = 200\,000 \text{ V/cm}$ and $\varphi = +\pi/2$ and a focused

laser beam, 1/500 the second-harmonic generation obtained with a KDP crystal under similar circumstances was observed. In calculating the relative values of the coefficients from this result, the angular spread of the laser beam must be considered, since $d\Delta k/d\theta$ for calcite at index match is ≈ 4 times that for KDP. Further, \mathbf{E}_{dc} was nonuniform. Considering these facts, we estimate

$$\begin{aligned} |(0.75c_{1122} + 0.24c_{3311}) - (0.47c_{3111} + 0.38c_{1311})| \\ (-2\omega_l, \omega_l, \omega_l, 0) \approx 3 \times 10^{-5} d_{36}(\text{KDP}) \text{ cm}^3/2 \text{ erg}^{-1/2}. \end{aligned}$$

A much larger value is expected here as \mathbf{E}_{dc} can induce ionic motion.

C. Three Wave Mixing Experiments

In this section measurements of the amount of radiation created at $\omega + \Delta$ due to the presence of radiation at ω and $\omega - \Delta$ are discussed. Because the total frequency spread 2Δ is much less than that for third harmonic generation 2ω , coherence lengths are much longer. With Δ small compared to ω , $l_{coh} \propto 1/\Delta^2$.

Figure 2 is a schematic of the experimental arrangement used. The laser beam was first focused with a 25-cm focal length lens into a 20-cm-long cell filled with a benzene derivative. Through Raman laser action and related interactions, the plane-polarized output beam contained frequency components at $\omega \pm n\Delta$, where n is an integer and Δ is a Raman frequency of the liquid. (See next section on Raman laser action at a focus.) Corning glass filters and an aperture stop were used to remove from this beam all frequency components except those at ω and $\omega - \Delta$. The power in the beam after these filters was 50 kW at ω , 10 kW at $\omega - \Delta$, 50 W at $\omega - 2\Delta$, and less than 10 photons per pulse at $\omega + \Delta$. The beam, after passing through a second focusing lens, was divided by a beam splitter into a reference channel and a sample channel. The samples were placed in front of the focus of the second lens so that the beam diameter within them could be directly measured. The light beams emerging from the samples were analyzed for radiation at $\omega + \Delta$ using grating monochromators and band pass dielectric filters. The filters with a band pass of 100 \AA were individually rotated to tune them to the

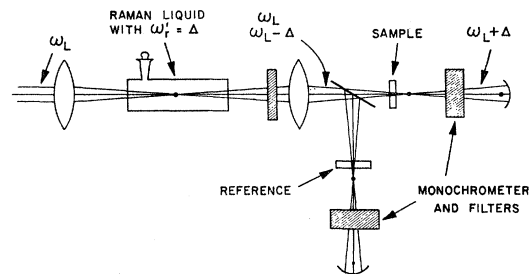


FIG. 2. Schematic of the experimental arrangement used to study the amount of radiation created at the frequency $\omega_l + \Delta$ due to the presence of waves at ω_l and $\omega_l - \Delta$.

³² R. W. Terhune, P. D. Maker, and C. M. Savage, Appl. Phys. Letters 2, 54 (1963).

³³ R. C. Miller, D. A. Kleinman, and A. Savage, Phys. Rev. Letters 11, 146 (1963).

³⁴ A. Ashkin, G. D. Boyd, and J. M. Dziedzic, Phys. Rev. Letters 11, 14 (1963).

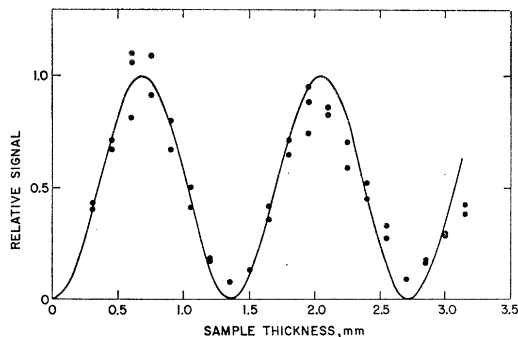


FIG. 3. The dependence on sample thickness of the signal at $\omega_l + \Delta_b$ created in benzene due to the presence of waves at ω_l and $\omega_l - \Delta_b$. The data illustrates the effect of the index mismatch and is fitted to a \sin^2 dependence.

desired wavelength. The signals from the photomultiplier detectors were combined through a delay line long enough to fully separate them, and displayed through the same oscilloscope channel. A thin piece of quartz remained in the sample position of the reference channel and all materials were measured relative to it. Pulse-to-pulse variations of the laser output, greatly magnified by two successive nonlinear processes, caused fluctuations as high as 5:1 in the signal from a single channel. The ratio between channels, however, remained constant to within 30%.

Equation (30) describes the growth of the wave at $\omega + \Delta$ in isotropic media and, when suitably modified [see Eq. (12) and accompanying discussion], certain cubic crystals. The amount of radiation created at $\omega + \Delta$ was purposely kept much smaller than that initially at $\omega - \Delta$. Under these conditions both the radiation at ω and $\omega - \Delta$ could be assumed constant throughout the sample. That is, the loss in intensity due to creation of the waves at $\omega + \Delta$ and $\omega - 2\Delta$ as well as the creation of additional radiation at $\omega - \Delta$ could be neglected.

A variable thickness liquid cell designed for spectroscopic applications was used for the study of liquids. Glass cover slips 0.006 in. thick were used as windows. Figure 3 shows typical data obtained with benzene as the cell thickness was scanned. The period of oscillation, or $2l_{\text{coh}}$, used in drawing the sine curve is just slightly less than that calculated from index of refraction data for the process described by Eq. (30). Most of the observed damping of the oscillations apparent in the data can be accounted for by the fact that the cell was in a convergent beam. Only a small fraction of the amount of radiation observed at the minima can be explained in this way, however. Possible explanations for the remainder include: creation of radiation at $\omega + \Delta$ due to the interaction of the three components at $\omega - 2\Delta$, $\omega - \Delta$, and ω , which has a markedly different l_{coh} ; imperfect overlap of the beams at ω and $\omega - \Delta$; or to collection of radiation at $\omega + \Delta$ generated at an angle

to the laser beam (see section on Raman laser action at a focus).

In studying liquids one needs to correct for the frequency mixing which occurs in the windows. This effect was minimized by using thin windows and making all quantitative measurements with the distance between the center of the two windows one coherence length. If conditions were ideal, the mixing in the first window would then completely cancel out that in the second.

Figure 4 shows the observed dependence of the total radiated signal upon the angle θ for a magnesium oxide sample one coherence length thick, again with benzene as the generating liquid. Also shown is the dependence predicted by a modified version of Eq. (12) with

$$\left[\frac{c_{1111}}{2c_{1122} + c_{1221}} \right] (-\omega_l + \Delta_b, \omega_l, \omega_l, -(\omega_l - \Delta_b)) = 0.61 \quad \text{or} \quad -0.27,$$

assuming the ratio to be real. By checking the direction of polarization of the signal at $\theta = 22\frac{1}{2}^\circ$, these alternative choices could be distinguished and the former value was found to be correct. Similar behavior was found in all the cubic materials studied except potassium chloride, for which the observed anisotropy was about equal to experimental error. The result implies that the third-order polarizability is greatest with \mathbf{E} along a $\langle 111 \rangle$ axis. Of interest is the qualitative observation that these materials also break down more easily with \mathbf{E} in this direction.

Simultaneous measurements of the intensities at $\omega_l, \omega_l - \Delta$ and $\omega_l + \Delta$ were made in an attempt to calculate the magnitude of the coefficients. The result for benzene was a factor of 8 less than that predicted from Raman scattering data. The calculation, however, assumed plane parallel overlapping waves (in both time and space) at ω_l and $\omega_l - \Delta$. Since the output signal at

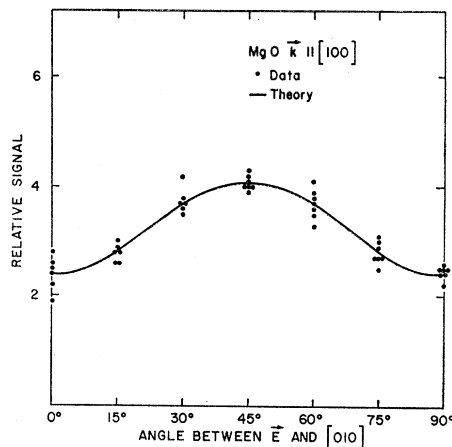


FIG. 4. Relative signal at $\omega_l + \Delta_b$ created by interaction of waves at ω_l and $\omega_l - \Delta_b$ in MgO as a function of sample orientation. θ was the angle between the (010) axis and $\mathbf{E}(\omega_l, r)$ which was parallel to $\mathbf{E}(\omega_l - \Delta_b, r)$. Propagation was along (100). Sample thickness was one coherence length, 1.27 mm.

TABLE I. Results of the three frequency mixing experiments with benzene ($\nu_b=992\text{ cm}^{-1}$) as the generator liquid. Data has been corrected for reflection losses and normalized so that for benzene $\chi_3'_{xxxx}[-(\omega_l+\Delta_b),\omega_l,\omega_l,-(\omega_l-\Delta_b)]=1.2\times 10^{-12}\text{ cm}^3\text{ erg}^{-1}$.

Material	$c_{1111}[-(\omega_l+\Delta_b),\omega_l,\omega_l,-(\omega_l-\Delta_b)]^a$ $\text{cm}^3\text{ erg}^{-1}\times 10^{14}$	$\frac{c_{1111}}{2c_{1122}+c_{1221}}[-(\omega_l+\Delta_b),\omega_l,\omega_l,-(\omega_l-\Delta_b)]$	l_{coh}^b mm
LiF	0.20 ^c	+0.74±0.10	3.27
KI	0.25	+0.54	0.45
CaF ₂	0.35	+0.66	2.94
MgO	1.0	+0.61	1.27 ^e
KCl	1.9	+1.10	0.92
NaCl	1.7	+0.78	0.88
KBr	3.0	+0.91	0.67
SrTiO ₃	d	+0.71	d
BSC Glass	1.3	a	2.04
Fused SiO ₂	0.7	a	1.45
C ₆ H ₅ CH ₃	4	a	0.80 ^e
C ₆ H ₅ Br	6	a	0.65
C ₆ H ₆	40	a	0.70
Quartz	1.0	a	1.67
CdS	d	a	d

^a For isotropic, trigonal and hexagonal materials, $c_{1111}=2c_{1122}+c_{1221}$ by symmetry.
^b From refractive index literature.

^c For a discussion of errors, see text.

^d See text.

^e Measured value.

$\omega_l+\Delta$ depends upon two successive nonlinear interactions, or intensity conversions, of the laser beam, it is not surprising that these approximations have broken down. In practice, that component of the nonuniform laser beam most effective in generating $\omega_l+\Delta$ has suffered the greatest attenuation in the creation of the wave at $\omega_l-\Delta$. The remainder is ineffective in either process, contributing only to the measured intensity at ω_l . Further it was observed that, owing probably to chromatic imaging errors, the beams at ω_l and $\omega_l-\Delta$ focused at slightly different points.

Because of these uncertainties, it was decided to normalize all coefficients to that predicted for benzene on resonance, $\chi_3'_{xxxx}[-(\omega_l+\Delta_b),\omega_l,\omega_l,-(\omega_l-\Delta_b)]=1.2\times 10^{-12}\text{ cm}^3\text{ erg}^{-1}$. Values thus deduced for the coefficients of various isotropic and cubic materials are given in Table I. Several materials of trigonal and hexagonal symmetry are also included. For these crystals, the direction of propagation was chosen parallel to the crystallographic optic axis so that the interaction was independent of further sample orientation. The values listed in column two have a relative precision of $\pm 20\%$ as inferred from the reproducibility of the results. A rather large error was assigned to the observed ratio of coefficients, given in column three, since the results, which were very consistent within a given sample, varied somewhat between samples.

The entry at column two for SrTiO₃ has been omitted. A sample 0.006 in. thick, which is about two coherence lengths, was used. Assuming the signal was about 1/10th that which would be observed for a sample one coherence length long, we would deduce a value of $400\times 10^{-14}\text{ cm}^3\text{ erg}^{-1}$. For CdS, a value of $160\times 10^{-14}\text{ cm}^3\text{ erg}^{-1}$ is deduced assuming the sample thickness, 0.0015 in., is less than a coherence length. The very large coefficients for these high refractive-index materials reflect the local-field correction discussed earlier, and when normalized are not surprisingly large. A two-

photon absorption resonance, as demonstrated later in SrTiO₃, may however also be contributing to these large coefficients.

By changing the Raman generating liquid in the experimental arrangement of Fig. 2, it was possible to change the difference frequency Δ and hence to measure the dependence of the χ_3 tensor components upon Δ . No appreciable changes were expected or found, except in those materials for which Δ is near a Raman resonance frequency, i.e., in the generating liquids themselves. Using benzene ($\nu_b=\Delta_b/2\pi;=992.4\text{ cm}^{-1}$), aniline ($\nu_a=996.8\text{ cm}^{-1}$), bromobenzene ($\nu_{bb}=1000.3\text{ cm}^{-1}$), benzonitrile ($\nu_{bn}=1001.6\text{ cm}^{-1}$), toluene ($\nu_t=1003.8\text{ cm}^{-1}$), and fluorobenzene ($\nu_f=1009.1\text{ cm}^{-1}$) as generators, the data of Fig. 5 was obtained. The frequencies just quoted were measured during studies of Raman laser action in these liquids. Measurements were also made using deuterated benzene ($\nu_{db}=945\text{ cm}^{-1}$) as a generating liquid. The following values of $|\chi_3'_{xxxx}$

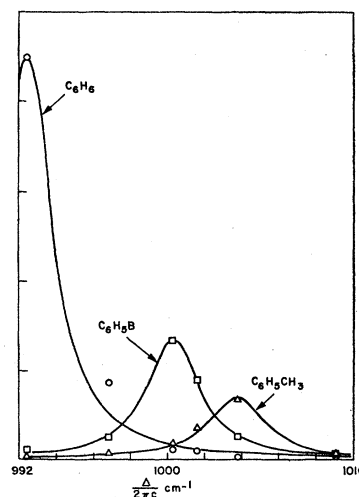


FIG. 5. Observed dependence of the amount of radiation created at $\omega_l+\Delta$ in various liquids. Different values of Δ were obtained by using a sequence of substituted benzenes as the generating liquids. Solid curves are Lorentzian line shapes fitted to the data.

$\times [-(\omega_l + \Delta_{db}), \omega_l, \omega_l - (\omega_l - \Delta_{db})]$ were obtained for the various liquids: benzene, $3.7 \times 10^{-14} \text{ cm}^3 \text{ erg}^{-1}$; bromobenzene, $5.1 \times 10^{-14} \text{ cm}^3 \text{ erg}^{-1}$; toluene, $3.4 \times 10^{-14} \text{ cm}^3 \text{ erg}^{-1}$. Here and in the previous experiments, several glass samples were compared to the quartz reference piece to verify that the reference signal was not frequency-dependent.

According to Eqs. (30) and (15), the observed line shapes should be determined by the square of the sum of a resonant part,

$$\chi_3^r \text{xxxx} [-(\omega_l + \Delta), \omega_l, \omega_l, -(\omega_l - \Delta)] \frac{\Gamma_r}{\omega_r' - \Delta - i\Gamma_r}$$

and a nonresonant part,

$$3\chi_3^{\text{nr}} \text{xxxx} [-(\omega_l + \Delta), \omega_l, \omega_l, -(\omega_l - \Delta)] \text{ of } 3\chi_3^{\text{xxxx}} [-(\omega_l + \Delta), \omega_l, \omega_l, -(\omega_l - \Delta)].$$

The nonresonant part is most likely real with an absolute value close to that obtained far from resonance with deuterated benzene as a generating liquid. Making this assumption, the ratio

$$\frac{3\chi_3^{\text{nr}} \text{xxxx} [-(\omega_l + \Delta), \omega_l, \omega_l, -(\omega_l - \Delta)]}{\chi_3^r \text{xxxx} [-(\omega_l + \Delta), \omega_l, \omega_l, -(\omega_l - \Delta)]}$$

is 1/20 for benzene, $\frac{1}{4}$ for bromobenzene, and $\frac{1}{6}$ for toluene. As the real part of the resonant contribution has a different sign above and below resonance, one would thus expect the wings of the observed lines to be asymmetric. This effect should be quite noticeable for bromobenzene and toluene.

The curves shown in Fig. 5 are Lorentzian-shaped resonance curves fitted to the data. The width for benzene is close to that observed in Raman spectra, while those for bromobenzene and toluene are about 50% greater. The data for bromobenzene and toluene show some asymmetry but not nearly the amount expected. Further, the ratio of the maximum values for benzene and toluene is 7/1 compared to only 4/1 observed in Raman spectra.²² Thus, there appear to be major discrepancies between this data and its interpretation. More controlled experiments are needed to clarify these points.

D. Nonlinear Complex Refractive Index

Several authors have reported observation of two photon absorption processes.^{23,35-41} These are described

³⁵ W. Kaiser and C. G. B. Garrett, Phys. Rev. Letters 7, 229 (1961).

³⁶ I. D. Abella, Phys. Rev. Letters 9, 453 (1962).

³⁷ W. L. Peticolas, J. P. Goldsborough and K. E. Rieckhoff, Phys. Rev. Letters 10, 43 (1963).

³⁸ R. G. Kepler, J. C. Caris, P. Avakian, and E. Abramson, Phys. Rev. Letters 10, 400 (1963).

³⁹ J. L. Hall, D. A. Jennings, and R. M. McClintock, Phys. Rev. Letters 11, 364 (1964).

⁴⁰ S. Singh and B. P. Stoicheff, J. Chem. Phys. 38, 2032 (1963).

⁴¹ J. J. Hopfield, J. M. Worlock, and Kwangjai Park, Phys. Rev. Letters 11, 414 (1963).

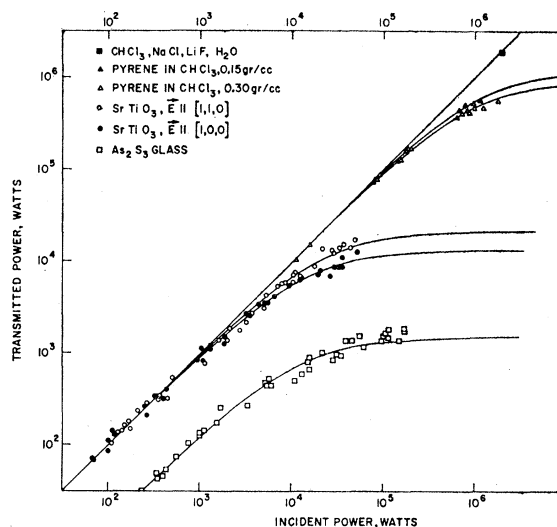


FIG. 6. Observed intensity-dependent absorption for several materials. The points represent data from individual laser pulses. Theoretical curves are fitted to the data. No nonlinear absorption was observed for those materials listed first.

by the imaginary part of the χ_3^4 two-photon resonance term of the induced polarization given in Eq. (13). As illustrated by Eq. (17), they can be thought of as resulting from an imaginary part of the intensity-dependent complex refractive index. When a light beam containing a single frequency is focused through a nonlinear material it is attenuated by this process in accordance with Eq. (33). Figure 6 shows the observed transmission to laser light of a group of materials having two photon resonances near 2ω , together with theoretical transmission curves fitted to the data. The cubic crystal strontium titanate in addition demonstrated an orientation-dependent effect, similar to that found for other χ_3 effects. The measurements were made by simply comparing the transmitted signal to a reflected fraction of the incident laser beam. In altering the laser intensity within the sample, calibrated glass filters were

TABLE II. Results of two-photon absorption measurements.

Material	$\text{Im}c_{1111}(-\omega_l, \omega_l, \omega_l, -\omega_l)^a$ $\text{cm}^3 \text{ erg}^{-1} \times 10^{14}$	W_m kilowatts
Pyrene, in CHCl_3		
0.15 gr/cc	0.24 ^b	1200
0.30 gr/cc	0.32	900
SrTiO_3	23 ^c	21
As_2S_3 glass ^d	110	5
CS_2	1.7 ± 1.2^e	
	0.7 ^f	

^a $c_{1111} = 2c_{1122} + c_{1221}$ in isotropic materials.

^b Estimated absolute error a factor of 2. Precision of the first four entries is ± 0.2 or $\pm 30\%$.

^c $\frac{\text{Im}c_{1111}}{\text{Im}(2c_{1122} + c_{1221})}(-\omega_l, \omega_l, \omega_l, -\omega_l) = 0.45$.

^d Data corrected for linear absorption.

^e Data from Giordmaine and Howe (Ref. 23).

^f Value for $\text{Im}[2c_{1122} + \frac{1}{2}c_{1221}](-\omega_l, \omega_l, \omega_l, -\omega_l)$ obtained using elliptically polarized light discussed later in text.

moved from in front of the sample to behind it without changing the light flux at the detectors.

The data tended to depart from the theoretical curves at high nonlinear attenuation, presumably because of the nonuniformity, both in time and space, of the laser beam. By extrapolation of the theoretical curves to infinite laser power, the maximum transmittable powers W_m were determined and from them values for $\text{Im}c_{1111}$ were computed using Eq. (33) with a degraded l/α ratio. These are summarized along with the data of Giordmaine and Howe²³ in Table II.

In a recent experiment by Hopfield, *et al.*⁴¹ the two-photon absorption spectrum of potassium iodide was obtained by studying its spectral transmission during illumination by a laser pulse. Decreases in the transmission at frequency ω_w during the laser pulse signify two photon resonance at frequency $\omega_w + \omega_l$. The optical arrangement did not permit accurate evaluation of the coefficients involved.

TABLE III. Results of measurements of intensity-dependent rotation of the vibrational ellipse and intensity induced birefringence.

Material	$\text{Re}c_{1221}(-\omega_l, \omega_l, \omega_l, -\omega_l)$ $\text{cm}^3 \text{erg}^{-1} \times 10^{14}$	$\text{Re}\frac{1}{2}(c_{1221} + c_{1212})(-\omega_w, \omega_w, \omega_l, -\omega_l)$ $\text{cm}^3 \text{erg}^{-1} \times 10^{14}$
H ₂ O	0.03 ^b	
CH ₃ OH	0.03	
C ₆ H ₁₄	0.09	
CCl ₄	0.12	
CHCl ₃	0.5	
CHBr ₃	0.7	
C ₆ H ₅ N	1.0	
CS ₂	4.5	40
C ₆ H ₆		7
C ₆ H ₅ NO ₂		30
C ₆ H ₅ COCl		30

^a From data of Mayer and Gires (Ref. 42) $\lambda_w = 5000 \text{ \AA}$.

^b Estimated absolute error a factor of 2. Precision of these measurements is ± 0.03 or $\pm 30\%$.

Measurements have also been made of intensity dependent changes in the real part of the refractive index. Mayer and Gires⁴² have studied the birefringence induced in a liquid by a plane-polarized laser beam. Due to lack of sensitivity, they were forced to use a broad band source in measuring the birefringence and could then detect effects only in materials having resonant coefficients. Ignoring two-photon absorption, their data can be interpreted in the terms of this paper using Eq. (27), and they are listed in Table III.

Intensity-dependent rotation of the vibrational ellipse of elliptically polarized laser light, as described by Eq. (23), has also been measured.²⁴ The experimental arrangement was as shown in Fig. 7. The laser output was first plane polarized, then elliptically polarized by a mica one-eighth wave plate whose fast and slow axes were bisected by the polarization vector of the laser beam. Using a right angle Rochon prism as an

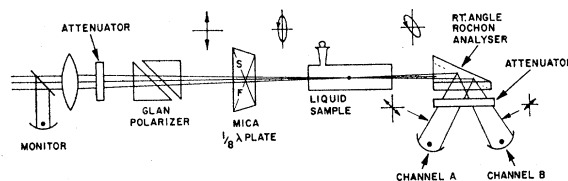


FIG. 7. Experimental arrangement used to detect intensity-dependent rotation of the vibrational ellipse. The state of polarization of the beam as seen when facing into the laser is indicated at several key positions. The rotation shown would result from a positive coefficient.

analyzer, the transmitted beam was divided into components plane polarized in the direction of the mica fast and slow axes. In the absence of rotation of the polarization vibrational ellipse, the powers W_A and W_B in these two components were equal. Actual data are shown in Fig. 8. The coefficient $\text{Re}c_{1221}$ was evaluated from the observed rotation using Eq. (23) and the fact that $W_A/(W_A + W_B) = \frac{1}{2}(1 + 0.707 \sin 2\alpha)$. These results are also given in Table III.

The study was confined to liquid samples as residual birefringence obscured the nonlinear effect in all of the crystal and glass samples on hand. Also, Raman laser action was encountered in all of the liquids save methanol and *n*-hexane. Data was recorded only at laser power levels at least 1 dB below the observed Raman laser threshold.

The coefficient $\text{Re}c_{1221}$ was found to be positive in all the liquids studied. Assuming $\text{Re}c_{1122}$ to have the same sign, this implies increased refractive index and Rayleigh scattering at high intensities.

The high value found for $\text{Re}c_{1221}$ in carbon disulfide reflects the two-photon absorption resonance observed by Giordmaine and Howe.²³ A 10% nonlinear absorption

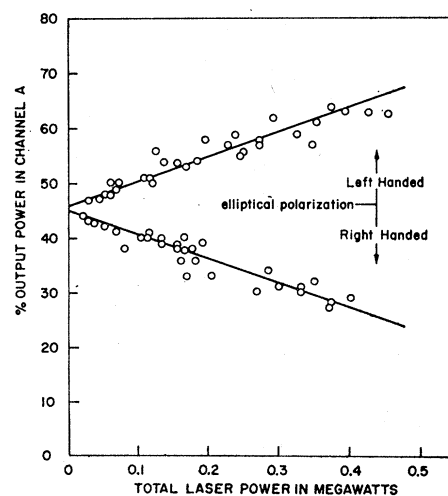


FIG. 8. Percentage of total transmitted power in channel A of Fig. 7 with a bromoform sample. The upper data was taken with the slow axis of the $\frac{1}{8}\lambda$ plate parallel to the plane of polarization detected by channel A. For the lower data, the mica was rotated 90°. Data points indicate the results of individual laser pulses.

⁴² G. Mayer and F. Gires, *Compt. Rend.* **258**, 2039 (1964).

was also noted at the highest laser powers used during our measurements of the rotation of the vibrational ellipse. This absorption did not interfere with the determination of $\text{Re}c_{1221}$ and from it we were able to deduce the value for $\text{Im}(2c_{1122} + \frac{1}{2}c_{1221})$ given in Table II. The positive sign of the coefficient $\text{Re}c_{1221}$ in this near-resonant case implies that $2\omega_l$ is less than the resonant frequency. This is further evidence for the assignment of the B_2 state resonant near 3200 \AA as that responsible for the enhanced coefficients.²³

Attempts were also made to measure the intensity induced birefringence in cubic crystals resulting from the $c_{1111} - (2c_{1122} + c_{1221})$ term [see Eq. (12)]. The poor optical quality of the available samples obscured the effect.

E. Raman Laser Action and Related Effects at a Focus

Figure 9 indicates the result of simply focusing a pulsed ruby laser into a liquid such as benzene.⁴³ A series of coaxial cones of light having a common apex at the laser focal point, and each of a different color, were observed to emanate from the sample. The ring pattern shown was produced by placing film behind the sample at right angles to the optical axis. The spectrum at the bottom of the figure was obtained by imaging such a ring pattern into a spectrograph with very wide entrance slits. The new frequency components were thus shown to be equally spaced by the frequency of the most intense Raman resonance of the liquid. Typical amounts of energy present in each of the various components, relative to that in the laser beam, are shown in Fig. 10.

The following explanation roughly accounts for the major features of this phenomena. The process is

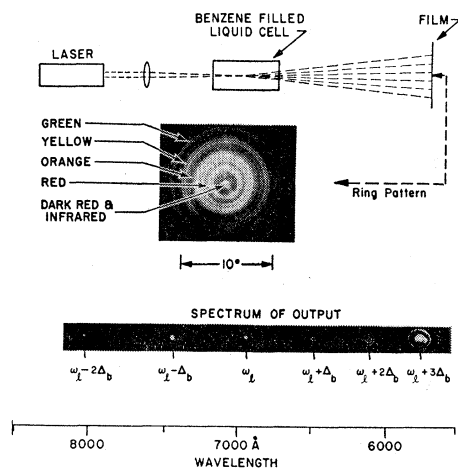


FIG. 9. Result of focusing a pulsed laser into benzene. A spectrograph with wide entrance slit produced the spectrum which shows the new frequencies to be separated by 992 cm^{-1} , the frequency of the strongest Raman line in benzene.

⁴³ R. W. Terhune, *Bull. Am. Phys. Soc.* 8, 359 (1963).

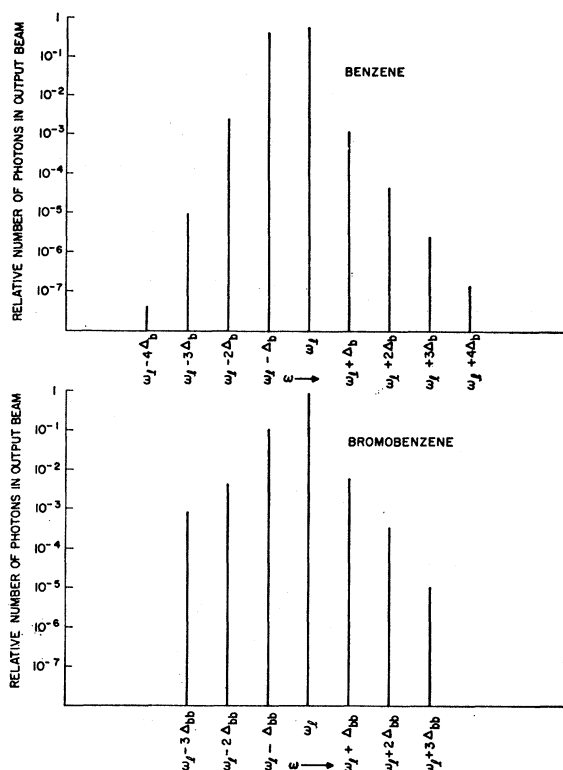


FIG. 10. Energy content of ring pattern produced as in Fig. 9. Data are results of averaging over many laser pulses of 10^9 W nominal peak power. Simultaneous weak Raman laser action in the 3064 cm^{-1} line of benzene was also usually observed.

initiated by the spontaneous Raman scattering at frequency $\omega_l - \Delta_b$ of $\sim 1:10^7$ per centimeter of the laser beam. Part of the scattered radiation passes through the focal region and is there amplified by Raman laser action as described by Eq. (25). For our laser pulse, independent of the focal length of the lens used, some 10^4 scattered photons will pass through the focus and be amplified, assuming the laser beam unattenuated, by e^{100} [see Eq. (35)]. Thus, the laser beam is attenuated as the beam at $\omega_l - \Delta_b$, the first Stokes frequency, is amplified. For the lenses used, the focal volume resembled a long slender cylinder and the gain at $\omega_l - \Delta_b$ was sharply peaked for radiation travelling nearly parallel to the optical axis. Although this single pass amplification process seems adequate to explain the observations, feedback at $\omega_l - \Delta_b$ supplied by Rayleigh scattering or some other mechanism could possibly be large enough to sustain oscillations. Simultaneous with the creation of a wave at $\omega_l - \Delta_b$, a polarization is induced at $\omega_l + \Delta_b$, the first anti-Stokes frequency, and at $\omega_l - 2\Delta_b$, the second Stokes frequency, through the resonant interaction described by Eqs. (15) and (30). The radiation thus created at $\omega_l + \Delta_b$ emerges in certain preferential off-axis directions determined by the phase velocity mismatch. That at $\omega_l - 2\Delta_b$ is amplified by Raman laser action and emerges chiefly in the axial

direction. These radiations then interact with the beams, at ω_l and $\omega_l - \Delta_b$ to produce further Stokes and anti-Stokes frequencies.

Several papers, both theoretical and experimental have recently appeared on this subject.^{4,10,11,16,25,44-53} These include observation of the effect in solids and gases, as well as in liquids. We have also observed it in water which has a very broad Raman transition and consequently a highly unfavorable α_{01}^2/Γ_r ratio. This required at 5-mW laser pulse. Thus, the effect appears to be completely general and will occur if sufficient laser power is present in any transparent material having a transition of Raman symmetry at a frequency lower than that of the laser. The laser power threshold is, however, very sharp. A decrease of 1 dB is often enough to reduce to zero a formerly brilliant example of the effect.

It is very difficult to obtain quantitative information from these experiments because of the many different interactions which are simultaneously occurring. Any analysis is further complicated by the complex field distribution in the region of the focus. Thus, of the wide range of observations we have made, only a limited number will be discussed.

1. α_{01} from Threshold Measurements

As seen in Eq. (35), the Raman laser gain depends exponentially upon $(L\alpha_{01}^2/\Gamma_r)W(\omega)$. Hellwarth^{10,11} has found good agreement between the measured threshold power for Raman laser oscillations in a resonant cavity of known Q and that predicted using this gain expression and previously measured values for $L\alpha_{01}^2$ and Γ_r . For the case of a focused laser beam, the measurement of threshold laser power still gives a rough measure of $L\alpha_{01}^2/\Gamma_r$ even though the precise amplification mechanism (feedback oscillations or single pass gain) and parameters (feedback factor, loss, input signal) remain largely unknown. It will be assumed that a gain per traversal of the focus of e^{30} results in Raman laser action (certainly more than e^{10} and less than e^{100} is required). Using our previous assumptions, a threshold of ~ 300 KW is predicted for liquid benzene and 1 MW for gaseous H_2 at high pressures.

⁴⁴ E. S. Woodbury, *Quantum Electronics III*, edited by P. Grivet and N. Bloembergen (Columbia University Press, New York 1964) p. 1577.

⁴⁵ G. Eckhardt, R. W. Hallwarth, F. J. McClung, S. E. Schwarz, D. Weiner, and E. J. Woodbury, *Phys. Rev. Letters* **9**, 455 (1962).

⁴⁶ G. Eckhardt, D. P. Bortfeld, and M. Geller, *Appl. Phys. Letters* **3**, 137 (1963).

⁴⁷ M. Geller, D. P. Bortfeld, and W. R. Sooy, *Appl. Phys. Letters* **3**, 36 (1963).

⁴⁸ E. Garmire, F. Pandarese, and C. H. Townes, *Phys. Rev. Letters* **11**, 160 (1963).

⁴⁹ H. J. Zeiger, P. E. Tannenwald, S. Kern, and R. Herendeen, *Phys. Rev. Letters* **11**, 419 (1963).

⁵⁰ R. Chiao and B. P. Stoicheff, *Phys. Rev. Letters* **12**, 290 (1964).

⁵¹ B. P. Stoicheff, *Phys. Letters* **7**, 186 (1963).

⁵² G. Bret and G. Mayer, *Compt. Rend.* **258**, 3265 (1964).

⁵³ N. M. Kroll, *Phys. Rev.* **127**, 1207 (1962).

The threshold in hydrogen was measured to be 1.5 MW. The result was reproducible from laser shot to shot within 1 dB. Threshold measurements in benzene and other liquid samples were, however, reproducible to within only about 4 dB. The threshold for benzene was near that predicted.

Also, using our models, the threshold for Raman laser action should be independent of the beam convergence. Using different lenses, the convergence was varied by a factor of 10. No change in threshold for benzene to within a factor of two could be detected.

Measurements were made to determine the polarization state for which Raman laser action occurred in H_2 with different states of polarization of the input laser beam. The polarization states for the two beams were found to be the same within experimental error. That is, with the laser beam elliptically polarized, the Raman laser beam was observed also to be elliptically polarized with the same eccentricity and sense. Further, the threshold for Raman laser action was observed to be independent of the polarization state of the laser beam.

The polarizability matrix elements in the space fixed system for the various vibration rotation transition of H_2 , $\langle g|\alpha_{ij}|r\rangle$, [see Eq. (14)] have been measured with good precision.^{54,55} The results are tabulated in terms of α_{01} , the isotropic part, and γ_{01} , the anisotropic part of the polarizability matrix element for the vibrational transition in the molecule fixed coordinate system. $\langle g|\alpha_{ij}|r\rangle$, $i \neq j$ contains contributions only from γ_{01} .⁵⁵ For pure vibrational transitions, $\Delta J=0$, an error of the order of only 2% in the intensities in Raman spectra is made in neglecting γ_{01} . Therefore, it is reasonable to assume $\gamma_{01}=0$ which implies $c_{1122}=c_{1221}=0$ [see Eqs. (10) and (14)]. The above experimental observations on polarization state and threshold for Raman laser action are predicted if one assumes $c_{1122}=c_{1221}=0$.

The threshold for Raman laser action in molecular vibration rotation transitions of diatomic molecules with $\Delta J \neq 0$ is predicted to be polarization dependent. With the laser beam circularly polarized, the threshold should be 2/3 that for the laser plane polarized. This dependence should be observed with Raman laser action in pure rotational transitions, $\Delta J=2$, which are the most intense transitions in gaseous N_2 at low temperatures.

2. Front to Back Ratio

The theory for Raman laser action discussed so far predicts the gain to be independent of the relative directions of the two beams when they are both polarized in the same direction [see Eq. (25)]. Thus, one of our first experiments on Raman laser action at a focus was to measure the ratio of the radiation at $\omega - \Delta$ emerging in the forward (parallel to the laser beam) and reverse

⁵⁴ R. W. Terhune and C. W. Peters, *J. Mol. Spectr.* **3**, 138 (1959).

⁵⁵ C. Church, thesis, University of Michigan, 1959 (unpublished).

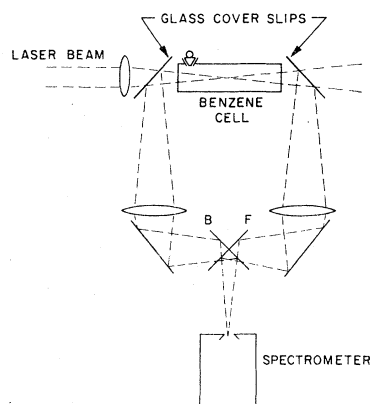


FIG. 11. Experimental arrangement used in measuring the forward to backward ratio for Raman laser action.

(antiparallel) directions. The experimental set up used is shown in Fig. 11. Only a limited number of observations were made, but it was shown that, at the laser powers available, the anti-Stokes radiation emerged only in the forward direction and the Stokes radiation emerged predominantly in the forward direction. For benzene, where Raman laser action occurred at the two displacement frequencies $\Delta_{b_1}=992\text{ cm}^{-1}$ and $\Delta_{b_2}=3064\text{ cm}^{-1}$, the ratio of the front to back radiation for the lines $\omega_l-\Delta_{b_1}$ and $\omega_l-2\Delta_{b_1}$ is about 2:1, while the radiation at $\omega_l-\Delta_{b_2}$ was only in the forward direction. There appeared to be an interaction between the lines at $\omega_l-\Delta_{b_2}$ and $\omega_l-3\Delta_{b_1}$. In the forward direction the intensity of the line at $\omega_l-3\Delta_{b_1}$ was anomalously large, being greater than that at $\omega_l-2\Delta_{b_1}$, and the same as that at $\omega_l-\Delta_{b_2}$. This anomaly did not occur in the reverse direction. All of the ratios varied considerably from laser pulse to pulse, the data quoted being an average over many pulses. A definite asymmetry in the forward and reverse directions which varies for different resonances in the same material is illustrated.

There is much less transfer of momentum to the material for a forward scattering process than for reverse scattering. Bloembergen and Shen^{4,5,6} have pointed out that the relaxation of the vibrational excitation, expressed in terms of optical phonons, can be momentum-dependent, thus explaining the observed asymmetry. This would predict differences in the linewidth, and correspondingly in the peak intensity, of the forward and reverse spontaneous Raman scattering. As part of our program, C. W. Peters has carried out such a measurement, using an arrangement similar to that of Fig. 11, but with the laser replaced by a cooled mercury-arc source. A 1-m-long, 2-cm-diam liquid cell was used which trapped both the exciting and scattered radiation by total internal reflection. He found no differences in the peak intensity or width of the forward and reverse scattering for either the 992-cm^{-1} line or the 3064-cm^{-1}

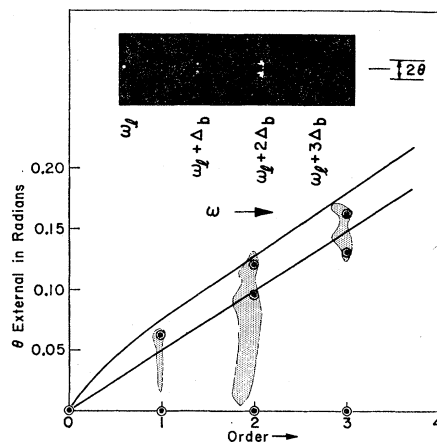


FIG. 12. Picture of spectrum obtained by imaging ring pattern from benzene on slit of spectrometer. The shaded areas of the plot indicate angles and frequencies at which radiation was observed in a series of laser pulses. The heavy dots indicate ring patterns obtained near threshold. The curves indicate predicted ring diameters using simple models.

line of benzene. The measurements had a precision of $\pm 5\%$ and thus are the most accurate that have been made. As the peak scattering power appears as an exponent in the expression for the Raman laser gain, a 5% difference would be very significant. Thus, the above measurements are still not definitive.

3. Angular Distribution and Frequency Spread of the Various Components

At the top of Fig. 12 is a photograph of a spectrum taken with the ring pattern imaged upon the narrowed entrance slits of the spectrograph. The spectrum thus reveals the angular distribution of the radiation as a function of frequency. It shows that the second and third anti-Stokes lines can comprise a very broad band of frequencies up to 100 cm^{-1} wide. In contrast, the corresponding spontaneous Raman linewidth is approximately 2 cm^{-1} . Within this 100-cm^{-1} region, the cone angles vary with frequency in a complicated fashion. Also, the frequency spread is seen to be predominately toward lower frequencies. Spectra taken with the laser power much closer to threshold, however, showed weak anti-Stokes lines which were very sharp in frequency and which formed well-defined cones. Similar spectra from gases such as H_2 and D_2 , where no rings are observed, show, even at the highest available laser power, little if any broadening of the anti-Stokes lines.

The plot shown at the bottom of Fig. 12 summarizes the anti-Stokes radiation patterns observed from benzene, showing the angle at which radiation emerges, measured from the laser axis, as a function of its frequency. The outlined regions are those in which radiation has been observed at maximum laser power levels.

⁵⁶ N. Bloembergen and Y. R. Shen, Phys. Rev. Letters **12**, 504 (1964).

The heavy dots represent the ring patterns observed at threshold. Also shown are curves corresponding to the radiation patterns of some simple models. The abscissa is one of these curves and is seen to predict axial radiation correctly. It corresponds to the case in which the transverse but not the longitudinal components of the phase velocities of the interacting waves sum to zero. This condition is required by a pancake-shaped polarization distribution but also describes radiation from a slab of polarization whose thickness is an odd-integral number of coherence lengths. The outer curve, which roughly predicts the outer set of threshold rings, corresponds to the opposite extreme, a line distribution, which requires that the longitudinal, but not the transverse, components of the phase velocities sum to zero. It is coupled to a model in which the axially propagating fields at ω_l and $\omega_l - \Delta_b$ combine with the axially propagating component of the field at $\omega_l + (n-1)\Delta_b$ to induce a polarization at $\omega_l + n\Delta_b$ through a resonant coefficient as described for $n=1$ by Eq. (15). The remaining curve, which roughly accounts for the second set of observed rings, corresponds to a resonant four wave interaction in which the vector sum of the phase velocities is zero. The process utilizes only that small fraction of the $\omega_l - \Delta_b$ beam which is propagating off axis at the angle required for phase matching. It thus predicts rings, of *reduced* intensity, at these angles in the radiation pattern at $\omega_l - \Delta_b$. Attempts to detect them have been unsuccessful. This process, including observation of the $\omega - \Delta$ rings, has however been identified by Chiao and Stoicheff⁵⁰ in calcite.

The Stokes radiation patterns, to the sensitivity available, consisted of a single axial lobe with about the same width as the laser beam. The radiation at $\omega_l - n\Delta_b$, $n \neq 1$, is probably the result of Raman laser amplification of the radiation from the polarization induced by the resonant three wave interaction involving the product $E^*(\omega_l, r)E(\omega_l - \Delta_b, r)E[\omega_l - (n-1)\Delta_b, r]$.

In many instances, rings occurred in doublet pairs, as illustrated by the outer members of the patterns shown in Fig. 3. Bloembergen and Shen^{4,56} have suggested that this results from an interference between two simultaneous processes which vanishes when they depart from the phase matched condition.

Although the simple models used above qualitatively describe the radiation patterns observed from liquids, they fail to give accurate predictions. A more refined analysis must consider, simultaneously, these simplified interactions and in addition several others such as intensity dependent changes in the refractive indices and stimulated Brillouin scattering.^{56,57} Although the large intensity-dependent changes in refractive index associated with the Raman resonance itself are zero when

$\delta\omega \equiv \omega_r' - \Delta$ is zero, they become very significant when $\delta\omega \simeq \Gamma_r$. As has been shown, even nonresonant changes are appreciable and these will measurably affect the phase matching angles. Additionally, more sophisticated handling of the complicated spatial distribution is required.

4. Nonresonant Creation of a Ring Pattern

In another experiment, the laser was first focused into a benzene cell so as to obtain Raman laser action. The axial components which emerged, as limited by an aperture stop, were then refocused into a cell containing nitrobenzene. The light emerging from this cell contained, in addition to rings at such combination frequencies as $\omega_l - \Delta_b + 2\Delta_{nb}$ and $\omega_l + \Delta_b + \Delta_{nb}$, a ring at frequency $\omega_l + 2\Delta_b$. This ring was formed through a *nonresonant* interaction since the nitrobenzene resonance differed markedly from that of benzene.

V. DISCUSSION

The experiments reported here are but a few of the many different ways that the spectrum of the third-order polarizability tensor can be studied using coherent processes. The relative values of coefficients determined in a given experiment appear to be reliable. However, there is considerable uncertainty in determining absolute values and hence in comparing the results of different experiments. Most of these uncertainties are introduced through the nonideal characteristics of our laser beam.

Given a gas laser in the watt range, one should be able to study several of the effects associated with χ_3 . The creation of new frequency components through the mixing of beams should be easily detectable with this intensity. By using an optical cavity with 20% loss per traversal at both the laser frequency ω_l and Raman laser frequency $\omega_l - \Delta$, one should be able to obtain Raman laser action in liquids such as CS₂. Placing the Raman active material at a focus inside the cavity would further enhance this interaction.

Studies of the interaction of white light with a laser beam, as in the experiments of Hopfield⁴¹ and Mayer,⁴² appear promising for scanning the spectrum of χ_3 . Changes in the white-light spectrum produced by the presence of the laser beam reflect both the molecular Raman spectrum and the two-photon absorption spectrum. Such observations would thus be very useful in the study of materials.

The many processes occurring at the focus of a laser beam remain to be untangled. Further calculations of the type carried out by Bloembergen and Shen^{4,56} in which several interactions are considered simultaneously need to be made.

These nonlinear effects could well be used in new types of optical devices, particularly as higher power

⁵⁷ R. Y. Chiao, C. H. Townes, and B. P. Stoicheff, Phys. Rev. Letters **12**, 592 (1964).

lasers become available. Moreover, the ever-present nonlinearities must be considered in developing such lasers—particularly Raman laser action and two-photon absorption processes since they limit the power-handling capabilities of materials.

ACKNOWLEDGMENTS

The authors are indebted to R. W. Minck, G. W. Ford, and C. W. Peters for many helpful discussions and to C. M. Savage for help in conducting the experiments.

Surface Effects in the Mixed Superconducting State

P. S. SWARTZ AND H. R. HART, JR.

General Electric Research Laboratory, Schenectady, New York

(Received 26 August 1964)

Measurements of the critical transport current above H_{c1} in a variety of $\text{Pb}_{0.95}\text{Tl}_{0.05}$ samples reveal that the surface can support a large transport current in the mixed state when the magnetic field vector is aligned with the surface. When a geometry is chosen so that the magnetic field vector can be aligned with a single surface (e.g., a cylinder of triangular cross section), the critical currents of opposite polarities differ by over a factor of 3 when the magnetic field vector is parallel to a surface plane; partial rectification is thus observed. The larger critical current is always in a direction that indicates that magnetic flux crosses out of the surface of a type-II superconductor more easily than into the surface. The "anomalous peak effect" (a maximum in the critical current just below H_{c2}) is observed in annealed samples and is identified with the strength of the Saint-James-de Gennes surface film *below* H_{c2} because of the manner in which it is affected by a thin surface film of copper. The critical-transport-current results suggest that two separate mechanisms contribute to the surface transport current in the mixed state. One of these mechanisms is identified with the Saint-James-de Gennes surface film *below* H_{c2} ; the second is tentatively associated with a bulk penetration depth. We measured a mixed-state resistivity and separated the contributions from the surface and the bulk. The bulk mixed-state resistivity is found to be independent of the density of bulk defects.

I. INTRODUCTION

IT has been established that superconductivity in a type-II superconductor can persist above the Abrikosov¹ upper critical field H_{c2} in a thin surface layer.²⁻⁶ The critical field of this surface layer is sensitive to the angle the magnetic field vector makes with the surface. When the magnetic field vector is parallel to the surface being explored, superconductivity persists to $H_{c3} = 1.69H_{c2}$.⁶ As the magnetic field vector is turned out of the plane of the surface, the critical field is reduced rapidly, becoming equal to H_{c2} at 90° .

A second surface phenomenon has been predicted by Bean and Livingston.⁷ They calculate that the surface acts as a barrier to the nucleation of the mixed state at H_{c1} , delaying the entrance into the mixed state until

magnetic fields somewhat greater than H_{c1} . The work of DeBlois and DeSorbo⁸ and Joseph and Tomasch⁹ supports the Bean-Livingston prediction.

In this paper we explore various surface phenomena in the mixed state ($H_{c1} \leq H \leq H_{c2}$) and between H_{c2} and H_{c3} . Our more significant findings are: (1) The surface of a type-II superconductor is capable of carrying significant transport supercurrents in the mixed state when the magnetic field vector is parallel to the plane of the surface. (2) The magnitude of the critical surface transport current is sensitive to the polarities of the transport current and the magnetic field in a manner revealing that in a type-II superconductor magnetic flux crosses the surface more easily from within the sample than from without; partial rectification can occur in a superconductor (see *Note Added in Proof*). (3) The "anomalous peak effect"^{10,11} near H_{c2} (sometimes called

¹ A. A. Abrikosov, *Phys. Chem. Solids* **2**, 199 (1957).

² C. F. Hempstead and Y. B. Kim, *Phys. Rev. Letters* **12**, 145 (1964).

³ H. R. Hart, Jr. and P. S. Swartz, *Phys. Letters* **10**, 40 (1964).

⁴ G. Bon Mardion, B. B. Goodman, and A. Lacaze, *Phys. Letters* **8**, 15 (1964).

⁵ W. J. Tomasch and A. S. Joseph, *Phys. Rev. Letters* **12**, 148 (1964); M. Cardona and B. Rosenblum, *Phys. Letters* **8**, 308 (1964); S. Gyax, J. L. Olsen, and R. H. Kroppschot, *ibid.* **8**, 228 (1964); Myron Strongin, Arthur Paskin, Donald G. Schweitzer, O. F. Kammerer, and P. P. Craig, *Phys. Rev. Letters* **12**, 442 (1964); J. P. Burger, G. Deutscher, E. Guyon, and A. Martinet (unpublished).

⁶ D. Saint-James and P. G. de Gennes, *Phys. Letters* **7**, 306 (1964).

⁷ C. P. Bean and J. D. Livingston, *Phys. Rev. Letters* **12**, 14 (1964).

⁸ R. W. DeBlois and W. DeSorbo, *Phys. Rev. Letters* **12**, 499 (1964).

⁹ A. S. Joseph and W. J. Tomasch, *Phys. Rev. Letters* **12**, 219 (1964).

¹⁰ W. DeSorbo, *Rev. Mod. Phys.* **36**, 90 (1964); S. H. Autler, E. S. Rosenblum, and K. H. Gooen, *Phys. Rev. Letters* **9**, 489 (1962); J. F. Schenk, J. S. Willis, and R. W. Shaw, *Phys. Letters* (unpublished).

¹¹ T. G. Berlincourt, R. R. Hake, and D. H. Leslie, *Phys. Rev. Letters* **6**, 671 (1961); J. J. Hauser and R. G. Trenting, *Phys. Chem. Solids* **24**, 371 (1962); R. R. Hake and D. H. Leslie, *J. Appl. Phys.* **34**, 270 (1963); R. R. Hake, D. H. Leslie, and C. G. Rhodes, *Proceedings of the Eighth International Conference on Low Temperature Physics* (Butterworths Scientific Publications, Ltd., London, 1963), p. 342.

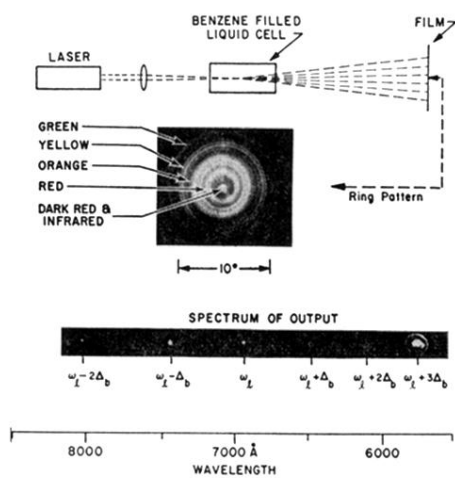


FIG. 9. Result of focusing a pulsed laser into benzene. A spectrograph with wide entrance slit produced the spectrum which shows the new frequencies to be separated by 992 cm^{-1} , the frequency of the strongest Raman line in benzene.